FH Aachen Campus Jülich

Faculty 3: Chemistry and Biotechnology

European Master in Nuclear Applications

FH AACHEN
UNIVERSITY OF APPLIED SCIENCES

Design and Construction of a stretched wire test bench to characterize Beam Position Monitor for the High Energy Storage Ring

Master Thesis by

Sudharsan Srinivasan

Jülich, July 2016

This work was carried out at Institute for Nuclear Physics (IKP – 4) in Forschungszentrum Jülich GmbH

This work was supervised by:

1. Prof. Dr. rer. nat Ulrich W. Scherer, FH Aachen

2. Dr. Vsevolod Kamerdzhiev, IKP – 4, Forschungszentrum Jülich

Declaration:

This thesis is my own independent work and is the result of my sole efforts. No other sources or references have been used in its production apart from the quoted ones.

Jülich, Date _____

Acknowledgment

I would like to express my gratitude to my supervisor Vsevolod Kamerdzhiev for the useful comments, remarks and engagement through the learning process of this master thesis. Furthermore I would like to thank Arthur Halama for introducing me to the topic as well for the constant support on the way. I would also like to thank Christian Böhme and Karl Reimers for lending me a helping hand whenever needed.

Also, I would like to thank Nils Giese from the Design Department of IKP-4 in helping to realize the test bench. I would also like to express my gratitude to Thomas Sefzick and the Electronics lab in IKP who constantly helped me in understanding related concepts.

I would like to express my deepest thanks and sincere appreciation to Prof. Ulrich W. Scherer for his constant support and belief. I would like to thank my parents and brother, who have supported me throughout entire process, both by keeping me harmonious, and helping me putting pieces together. I will be grateful forever for your love. I have to definitely thank my best friends Angel Saez Garcia and Deniz Avsar for sharing the same psychopathy. Last but not the least, I have to thank Liverpool FC for not letting me walk alone!

You'll Never Walk Alone!!!!!

Sud a.k.a. Sudharsan Srinivasan

Glossary

BPM	**Beam Position Monitor**
CMM	**Coordinate Measuring Machine**
COSY	**Cooler Synchrotron**
DAQ	**Data Acquisition**
DOS	**Difference Over Sum**
DUT	**Device Under Test**
EOS	**Electrical Offset**
FAIR	**Facility for Antiprotons and Ions Research**
FEA	**Finite Element Analysis**
HESR	**High Energy Storage Ring**
ZEA	**Central Institute for Engineering, Electronics and Analytics of the Research Center Jülich**

Table of Contents

Abstract

Accelerator physics is a branch of applied physics, which deals with design, construction and operation of particle accelerators. In today's world, their uses cover varied fields such as study structures in chemistry and biology or to perform sensitive trace element analysis. Moreover, accelerators have become entrenched as the key tools in the study of subatomic particles. Whether the application is scientific, industrial or medical, beam diagnostics is an essential constituent of an accelerator. This deals with the design and operation of instrumentation devices for monitoring the beam properties. Without adequate beam diagnostics, achievement of beam for physics use would be impossible as the beam is sensitive to imperfections of the accelerator. A beam position monitor (BPM) is one such beam diagnostic device.

This project deals with diagonally cut capacitive pickup as this design was chosen for High Energy Storage Ring (HESR) due to its high linear response and high sensitivity. Prior to beam operation, it is necessary to characterize the BPM which involves: establishing a relationship between the measured beam position and the actual one. This is achieved with the help of a standalone test bench using stretched wire method. Therefore, a test bench is designed and constructed to calibrate the BPM. Followed by which, a software/application is developed which can perform automated linearity tests. Linearity tests are carried out for two test configurations namely high particle intensity i.e. 10^{10} particles and low particle intensity i.e. 10^{8} particles.

For both test configurations, positional accuracy could be measured successfully within the requirements of the project which is 100 µm for 10^{10} particles and 1 mm for 10^{8} particles, for turn by turn detection. However, there is a considerable influence of noise signals on the uncertainties of the measurement itself. Their effects could be minimized by averaging over a considerable amount of revolutions.

Moreover, for approving the series production of HESR BPMs, single turn detection measurement will be carried out on the test bench. This mode of operation aims for beam injection optimization where a resolution of 1 mm is expected with particle intensities of 10^{7} and 10^{8}.

1. Introduction

1.1. Particle Accelerators

One of the most versatile instruments designed by physicists are particle accelerators. From its very first inception, as cathode ray tube by J.J. Thompson, till the present day large colliders, it is closely associated with major discoveries in nuclear and particle physics.

From 1959 till now, accelerators and colliders have allowed physicists to gain three orders of magnitude 100 GeV energy in their quest for probing matter at an increasingly finer scale [1]. In today's world, it is an essential instrument widely used not only in many field of physics but also to study structures in chemistry and biology or to perform sensitive trace element analysis. In the field of astrophysics and cosmology, accelerators are becoming more complementary to telescopes. In nuclear physics, accelerators are an essential tool to probe the nucleus, determine its structure and behavior [2]. Historically the development of particle accelerators took place in two major guidelines namely energy frontier and intensity frontier. At the energy frontier, scientists build advanced particle accelerators such as Tevatron, or LHC to explore the Terascale. At the intensity frontier, scientists use facilities such as J-PARC to create intense beams of trillions of particles for neutrino experiments and measurement of ultra-rare processes in nature [3]. Machines like COSY [4] however doesn't belong to either of these. These are specialized accelerators for precision based experiments which is the reason for necessitating beam cooling [5].

1.2. FAIR – the future accelerator facility

The Facility for Antiproton and Ion Research (FAIR), as shown in Figure 1, is an international accelerator facility of the next generation under construction in Darmstadt. The experimental requirements concerning particle intensities and energies will be met by the SIS100/300 double synchrotron with a circumference of about 1,100 meters and with magnetic rigidities of 100 and 300 Tm, respectively [6]. The goal of the SIS100 is to achieve intense pulsed ($5*10^{11}$ ions per pulse) uranium beams (charge state q = 28+) at 1 GeV/u and intense ($4*10^{13}$) pulsed proton beams at 29 GeV. The SIS300 will provide high-energy ion beams of maximum energies around 45 GeV/u for Ne^{10+} beams and close to 35 GeV/u for fully stripped U^{92+} beams. The maximum intensities in this mode are close to $1*10^{9}$ ions/s. Connected to the facility will be a system of cooler-storage rings with beam

cooling, internal targets and in-ring experiments. The system of storage–cooler rings allows the quality of these secondary beams to be drastically improved. The Collector Ring (CR) will be used for stochastic cooling of radioactive and antiproton beams [6]. The Accumulator Ring (RESR) will be used for accumulation of antiproton beams after stochastic pre-cooling in the CR and also for fast deceleration of radioactive secondary beams with a ramp rate of up to 1 T/s [6]. The New Experimental Storage Ring (NESR) will be used for experiments with exotic ions and with antiproton beams. The NESR is equipped with stochastic and electron cooling [6]. The injector for the new facility will be the existing GSI accelerator SIS18 along with a planned proton-LINAC [6].

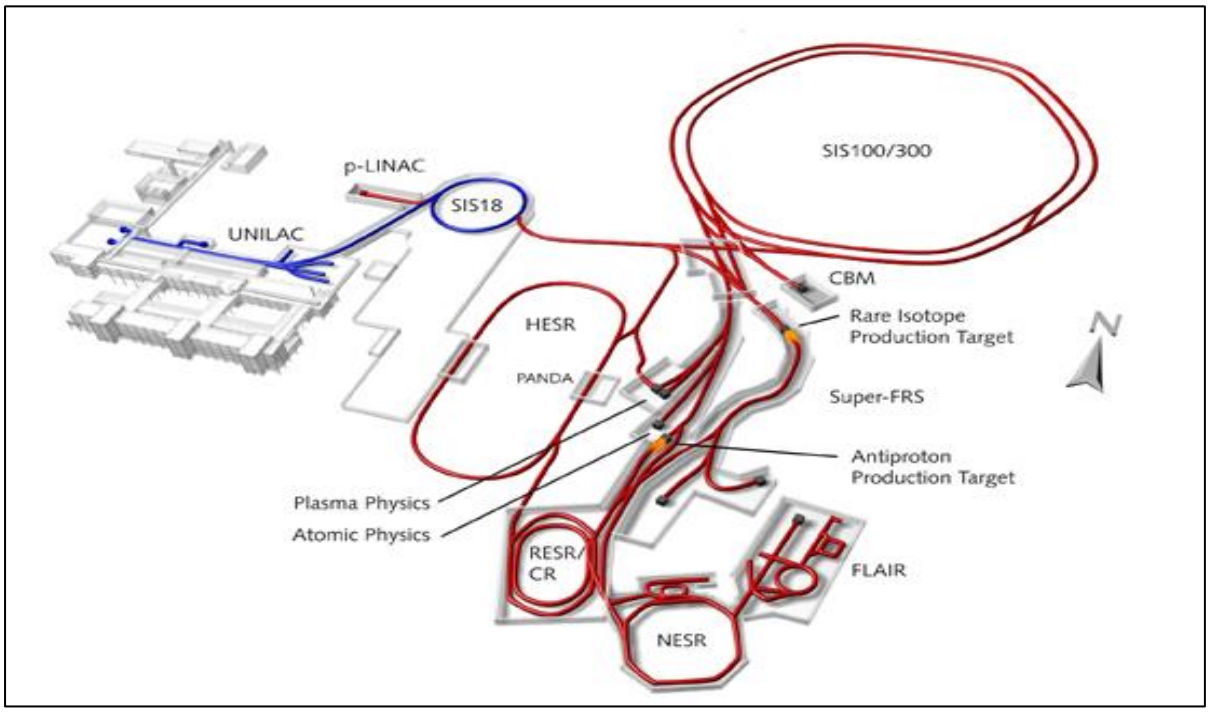

Figure 1: FAIR at GSI: SIS 18, 100/300 = synchrotrons with bending powers of 18, 100 and 300 Tm, respectively; CR = Collector Ring; RESR = Accumulator Ring; NESR & HESR = low & high energy experimental storage rings, Super-FRS = Fragment Separator [5].

1.3. HESR

The HESR (High Energy Storage Ring) synchrotron, as shown in Figure 2, part of the FAIR project, is primarily dedicated to the field of high energy antiproton physics. It provides high quality beams over the broad momentum range from 1.5 GeV/c to 15 GeV/c to explore the research areas of hadron structure and quark-gluon dynamics [7]. In addition, a heavy ion mode of operation is envisaged. Ions up to fully stripped uranium can be provided for the experiments in the HESR.

The 575 meter long HESR is designed as a racetrack-shaped storage ring with a

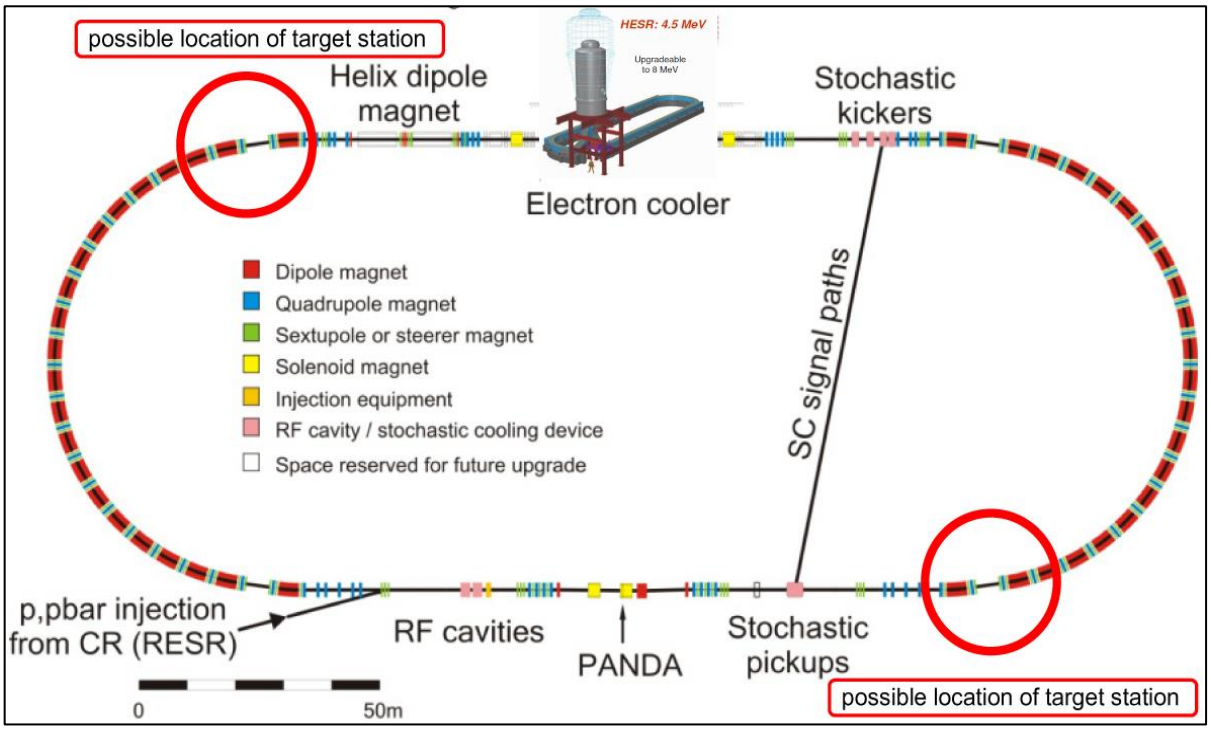

Figure 2: Schematic view of the HESR. Positions for injection, cooling devices and experimental installations are indicated [8].

magnetic bending power of 50 Tm. It consists of straight sections which are 132 meter long and of two arcs of 155 meter in length [8]. The inner diameter of the beam pipe is 89 mm, neglecting details in the region of the experiments and injection. According to the Modularized Start Version (MSV), injection of antiprotons will take place from the CR facility at particle energy of 3 GeV/c [8]. At a later stage the ring can be equipped with electron cooling up to an energy of 8 GeV (4.5 MeV electron energy maximum) and with stochastic cooling up to 15 GeV [8]. Moreover, a proton beam line for commissioning and, as a future option, for injection of polarized proton beams into the HESR from the SIS18 has been added.

An important feature of the new facility is the combination of phase space cooled beams with internal targets which opens new capabilities for high precision experiments. One of the straight sections will be used for installation of internal target and the sophisticated PANDA detector [9], and the other can be used to house beam cooling equipment. SPARC [10] and PAX [11] collaborations will also perform experiments at the HESR.

Figure 3 shows schematically beam time structure in the HESR with individual peaks representing beam bunches on a time domain i.e. time is abscissa. The time spacing between consecutive bunches represent the revolution time period where the ordinate is represented by intensity in arbitrary units. The bunch length will vary depending on beam conditions.

Various beam dynamics simulations have been accomplished to guarantee the required equilibrium beam parameters, beam lifetime and beam stability in HESR [12].

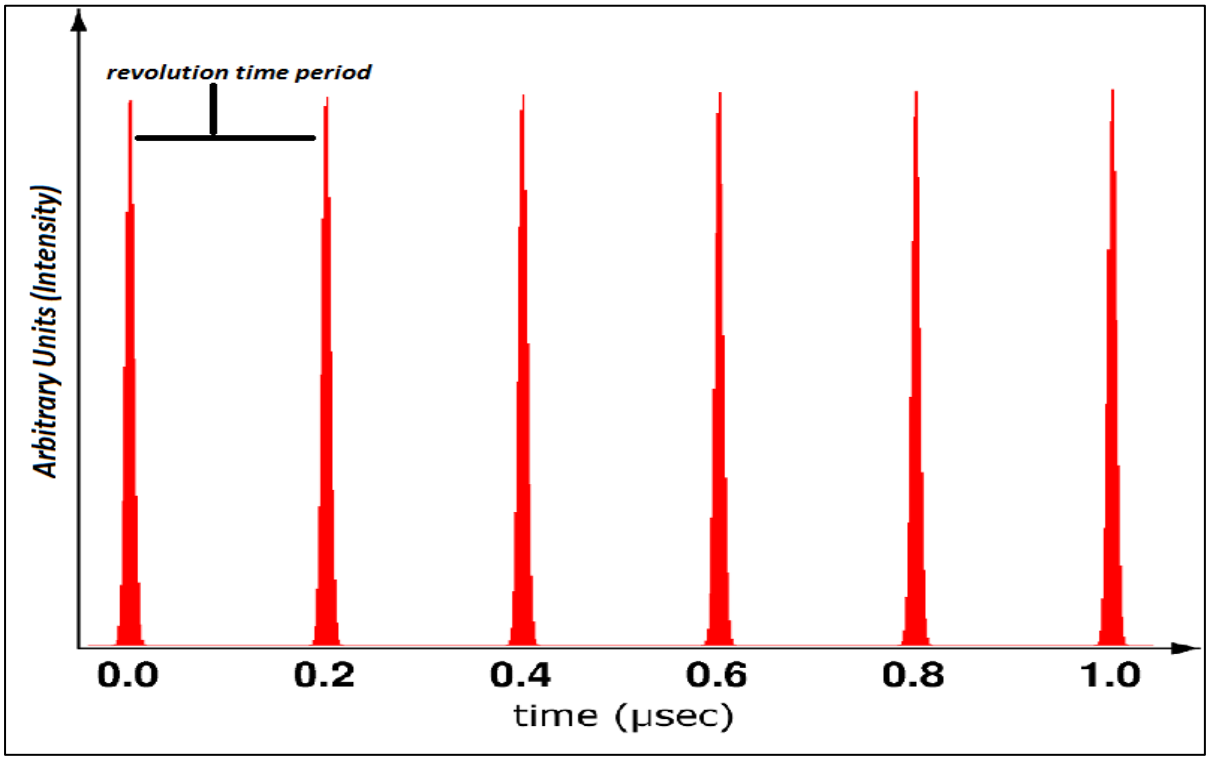

Figure 3: Typical beam time structure representation in the HESR.

2. Beam Diagnostics in Particle Accelerators

2.1. Introduction

Beam diagnostics is an essential constituent of an accelerator. This deals with the design and development of instrumentation devices for monitoring the beam properties. The beam diagnostic devices are placed along the beam line to project the beam properties in a form which can be processed. A device readout chain, usually integrated in a control architecture, acquires these signals, and delivers them to the control room main servers. These yield all beam parameter information displaying the characteristics and the behavior of the beam in the accelerator [13].

The following Table 1 lists some of the general beam diagnostic devices and the properties they can measure. Without adequate beam diagnostics, achievement of beam for physics use would be impossible as the beam is sensitive to imperfections of the accelerator. As a result, about 3% to 10% of the total cost of an accelerator facility is dedicated to diagnostic instrumentation [14]. However, due to the complexity in the design and technique involved, the amount of manpower for the design, operation, and further developments often exceed 10% [14]. Hence, there exists a vast choice of different types of diagnostic devices, each usually in many variants. One could classify these devices as electromagnetic, using secondary emission, etc., or as destructive and non-destructive. Many of these devices can measure more than one beam property and their variants may use different physical principles.

For closed orbit observation in circular accelerators, destructive type beam diagnostic devices are of no use. For example, in the HESR, the behavior of single pass as well as thousands of passages have to be determined. Henceforth, in a synchrotron, non-destructive methods are required to monitor the beam behavior without any modifying influences.

PROPERTY MEASURED →	Intensity/charge	transverse: Position	transverse: Size/shape	transverse: Emittance	longit.: Size/shape	longit.: Emittance	Q-value + ΔQ	Energy + ΔE	Polarization	Effect on beam: N	-	+	D
Beam transformers	●				●	●				x			
Wall-current monitors	●	●			●	●				x			
Pick-ups	●	●	●		●	●				x			
Faraday cup	●												x
Secondary emission monitors	●	●	●	●				•			x	x	
Wire scanners		●	●	●							x		
Wire chambers		●	●								x	x	
Ionization chambers	●										x	x	
Beam loss monitors		•	•	•			•			x			

Effect on beam: N none
- slight, negligible
+ perturbing
D destructive

● primary purpose
• indirect use

Only the most basic measured properties are shown. There are many more, less basic, which can be derived: coupling, dispersion, chromaticity, etc. Note that to determine emittance (transverse or longitudinal), knowledge other than that obtained from the basic measurement is required. The oscillatory behaviour of the beam is observed through the time-dependance of properties (like position, size/shape, energy), often on a very fast time scale.

Table 1: An outlay of basic diagnostic devices and beam properties measured [13]. The beam diagnostic device of concern for the study is pick-ups.

2.2. Overview of Beam Parameters

Beam Intensity

In a circular accelerator like the HESR, the intensity of charged particle beam is defined as the number of particles circulating in the ring. For a given revolution frequency, f_{rev}

$$I = N * Q * f_{rev} \quad (1)$$

The particle charge is Q, where N, is the number of particles. Having knowledge on beam current aids in determining the beam lifetime as the decay of its current [14].

Beam Position

For precise closed orbit determination, the beam's center position is measured at different locations in the ring over multiple turns. Some machine related studies require turn-by-turn measurement capability. Specifically, beam position is the center of charge within the transverse density distribution of the beam particles.

Beam profile

Transverse beam profiles are usually histograms representing the number of particles in a beam as a function of a transverse position [15]. Hence, we have a horizontal and vertical profile expressing the number of particles at different X and Y position. Considering 2D distributions, the profiles are simply the projection of 2D plots along one axis. Figure 4 shows a sketch of the different 2D distributions and relative profiles.

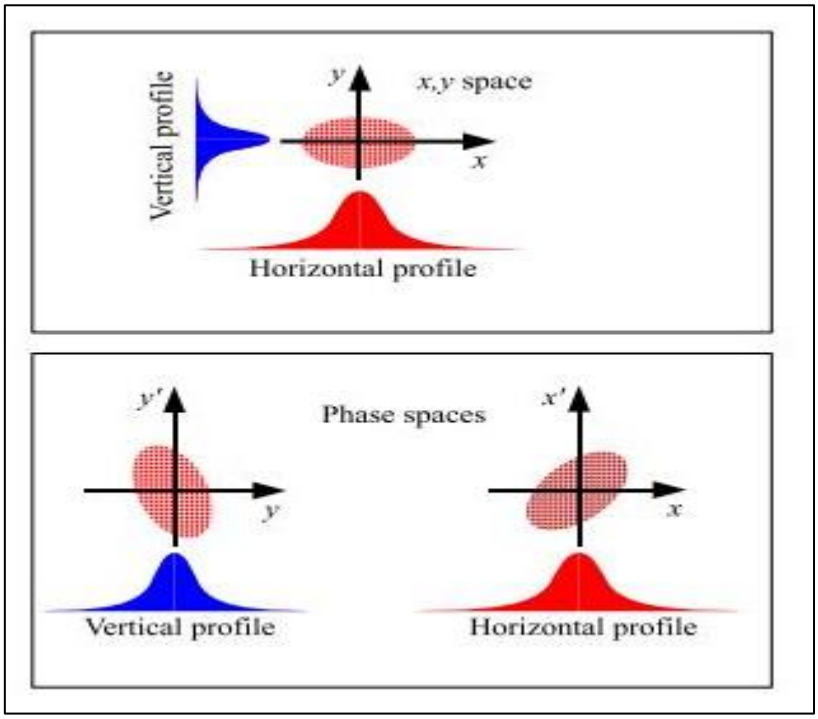

Figure 4: Different types of 2D distributions and relative transverse profiles: x, y transverse space (top left), transverse phase spaces (bottom left) [15].

2.3. Beam position measuring systems characteristics

In order to design a system that is simple and reliable but does not compromise on the quality of the measurements, it is important to understand how the system parameters affect the measurement results. Moreover, it is important to understand the requirements for the beam position monitoring systems before undertaking its detailed design, which are as follows [16]:

Position sensitivity: it is the proportional constant between the beam displacement and the pickup signal. It is defined as the $S_x(x) = \frac{d}{dx}\left(\frac{\Delta U_x}{\Sigma U_x}\right)$ in [%/mm] (linear) for the horizontal direction and for the vertical direction, correspondingly. For small displacements, it is a constant value. In our case, it is a function of horizontal and vertical beam displacements [16].

Accuracy: in general, accuracy of a system is the closeness of a measurement to its true value. For beam position measurement, it is the ability to measure the beam position relative to a defined transverse X, Y space. Its limitations are combination of pickup nonlinear response to displaced beams, mechanical alignment errors, calibration errors, electromagnetic interference and circuit noise. Signal processing introduces additional inaccuracies such as granularity due to analog to digital conversion.

Resolution: resolution in general refers to the smallest change a sensor can detect in the quantity it is measuring. Here, it is the ability to measure the smallest displacements of the beam.

Bandwidth: Analog bandwidth is the lower and upper cut-off frequency of the analog electronics that has to be matched to the frequency spectrum delivered by the bunched beam. **Acquisition bandwidth** is the frequency range over which the beam position is recorded and should be matched to the analog bandwidth. For real-time closed orbit control applications, a very small bandwidth is necessary whereas for turn-by-turn measurements, a much larger bandwidth is needed.

Dynamic range: dynamic range is the difference between the smallest and largest usable signal through a processing chain. Large dynamic range response is achieved by **gain adjustment.** Within the dynamic range, the position reading should have a negligible dependence with respect to the input level.

Signal-to-noise ratio: it is the ratio of the power level of the wanted signal relative to the level of unwanted noise. Noise can be true thermal noise, amplifier noise, EMI noise, RFI noise etc. Signal to noise ratio limits the ultimate resolution and accuracy of the measuring system.

Detection threshold: it is the minimal beam current for which the system delivers a usable information. It is limited by noise contributions.

2.4. Beam current modulation in the time and frequency domains

For bunched beams, beam bunching frequency is a provider of a carrier signal that can detect the beam position irrespective of the beam's shape. Since it is possible to make measurements in both time and frequency domain, it is important to understand the correlations.

Consider a Gaussian shaped beam bunch containing N particles of charge e in a bunch of rms temporal length σ (in time units) and with a bunching period T. The instantaneous current of a single bunch is given by [17]

$$I_b(t) = \frac{eN}{\sqrt{2\pi}} * \exp\left(-\frac{t^2}{2\sigma^2}\right) \tag{2}$$

This is normalized so that the bunch area is the total charge eN independent of the rms bunch length σ. Assuming the bunch to be symmetric in time centered at $t = 0$ and is in a pulse train with bunch spacing T, the above series can be expanded in a cosine series with $\omega_o = 2\pi/T$:

$$I_b(t) = \frac{eN}{T} + \sum_{m=1}^{\infty} (I_m \cos m\omega_0 t) \tag{3}$$

Where

$$I_m = \frac{2eN}{T} * \exp\left(-\frac{m^2 {\omega_o}^2 \sigma^2}{2}\right) \tag{4}$$

This can be rewritten as

$$I_b(t) = [I_b] + 2[I_b] \sum_{m=1}^{\infty} (A_m \cos m\omega_0 t) \tag{5}$$

Where the average (dc) beam current is

$$[I_b] = \frac{eN}{T} \tag{6}$$

And the harmonic amplitude factor A_m for harmonic $m\omega_o$ is

$$A_m = \exp\left(-\frac{m^2{\omega_o}^2\sigma^2}{2}\right) \tag{7}$$

The Fourier cosine series expansion of the equation (5) includes a dc component as well as many harmonics of the bunching frequency. The amplitude (intensity) of the various Fourier harmonics is determined by the factor A_m which always approaches 1 for small harmonic number irrespective of the bunch shape. For certain harmonic number m, the amplitude factor A_m can be zero depending on the bunch length [17]. In summary, the beam currents associated with periodically spaced bunches can be considered in both time and frequency domain.

For a beam centered in circular conducting pipe of radius b and with a velocity $\vartheta_b = \beta_b c$, wall current density is simply the beam current divided by the beam pipe circumference i.e. $i_W(t) = [-I_b(t)/2\pi b]$.

2.5. Signals from off-center beams

A centered beam inside a circular beam pipe was considered in the previous section 2.4. Now we consider a beam displaced from the center and investigate what happens to the wall current [17].

Laplace's equation can be solved in two dimensions to find the wall current density for a pencil beam current $I_b(t)$ at a position r, θ inside a grounded, circular, conducting beam pipe of radius b. The wall current density i_w at $b,\ \phi_w$ is then

$$i_w(b, \phi_w, t) = \frac{-I_b(t)}{2\pi b}\left[1 + 2\sum_{n=1}^{\infty}\left(\frac{r}{b}\right)^n \cos n(\phi_w - \theta)\right] \tag{8}$$

An alternative way to obtain a solution is to use the method of images. In this, the location of an image pencil beam is found such that the potential everywhere on the circle corresponding to the beam pipe (without the beam pipe) is zero. The wall current is then calculated by using the differential form of the Gauss Law. The resultant is the expression for the wall current density i_w at $b,\ \phi_w$ is

$$i_w(b, \phi_w, t) = \frac{-I_b(t)}{2\pi b}\left[\frac{b^2 - r^2}{b^2 + r^2 - 2br\cos(\phi_w - \theta)}\right] \tag{9}$$

This closed form-expression which is equivalent to the infinite series form, is sometimes easier to deal with than the infinite series. Note that the infinite series is of the form $r^n cos\, n\theta$, indicative of solutions in cylindrical geometry.

If two electrodes (L and R for left and right) of angular width ϕ_o are placed at 0° and 180° as shown in Figure 5, the resultant current flowing parallel to the beam on the inside surface of these electrodes are (assuming they are grounded and also at radius b)

$$I_R(t) = \frac{-I_b(t)\phi_o}{2\pi}\left\{1 + \frac{4}{\phi_o}\sum_{n=1}^{\infty}\frac{1}{n}\frac{r^n}{b}\cos n\theta \sin\frac{n\phi_o}{2}\right\} \tag{10}$$

$$I_L(t) = \frac{-I_b(t)\phi_o}{2\pi}\left\{1 + \frac{4}{\phi_o}\sum_{n=1}^{\infty}\frac{1}{n}\frac{r^n}{b}\cos n\theta \sin n\left(\pi + \frac{\phi_o}{2}\right)\right\} \tag{11}$$

We can now write the normalized (to beam current) difference-over-sum ratio for a displacement $x = rcos\theta$ as (where $R = I_R(t)$ and $L = I_L(t)$)

$$\frac{R-L}{R+L} = \frac{4\sin\frac{\phi_o}{2}}{\phi_o}\frac{x}{b} + higher\ order\ terms \tag{12}$$

A more linear approximation (in x) in cylindrical geometry is to write the ratio of R/L in decibels (i.e., logarithmic form)

$$20\log_{10}\frac{\mathrm{R}}{\mathrm{L}} = xS_x = \frac{\sin\frac{\phi_o}{2}}{\phi_o}\frac{x}{b} + higher\ order\ terms \tag{13}$$

The pickup displacement sensitivity S_x depends on both the in-plane and orthogonal-plane displacements. With the positions x and y measured, the in-plane non-linearity and orthogonal plane non-linearity can be corrected by using a software algorithm or look-up table. Both the equations (12) and (13) of the electrode response to the beam displacement have higher-order terms and are therefore nonlinear [17]. The nature of nonlinearities are different as equation (12) represents normalized amplitude difference and equation (13) represents the logarithmic ratio. An electrode shape can be designed that is linear in the normalized difference.

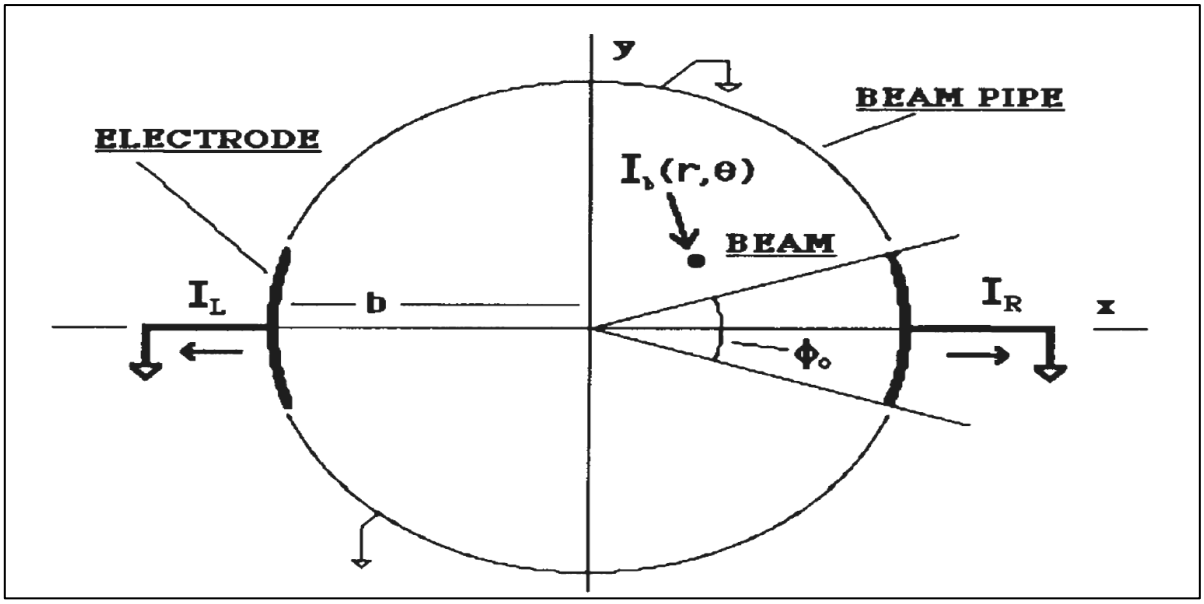

Figure 5: Cross section of Beam Position Monitor used for calculations [17].

2.6. Electrostatic pickup electrodes

To understand the response of electrostatic pickups (also called capacitive), we must first consider two opposing electrodes of length l and azimuthal width ϕ_o in a beam pipe of radius b. If the current of a centered pencil beam is $I_b(t)$ and the beam has velocity $v_b = \beta_b c$, the charge density of the beam is [17]

$$q_b(t) = \frac{I_b(t)}{\beta_b c} \tag{14}$$

On the inside surface of the electrode there appears an equal magnitude, opposite polarity charge. For an electrode of length l and azimuthal width ϕ_o, this charge is

$$Q_s(t) = \frac{-\phi_o l}{2\pi}\frac{I_b(t)}{\beta_b c} \tag{15}$$

As there is a capacitance between the electrode and the ground plane, the signal current flowing onto the capacitance is equal to the time derivative of the charge on the electrode:

$$i_s(t) = \frac{-dQ_s(t)}{dt} = \frac{\phi_o l}{2\pi}\frac{1}{\beta_b c}\frac{dI_b(t)}{dt} \tag{16}$$

Note that there is no dc component of the charge on the electrode. The capacitance C integrates the ac current, yielding an output voltage

$$V_c(t) = \frac{\phi_o l}{2\pi C}\frac{I_b(t)}{\beta_b c} - V_0 \tag{17}$$

Where V_0 is a constant of integration corresponding to initial voltage at t, time equals zero.

This capacitance may be directly between the electrode and the beam pipe, or it may be added externally [17]. The equivalent circuit is show in Figure 6.

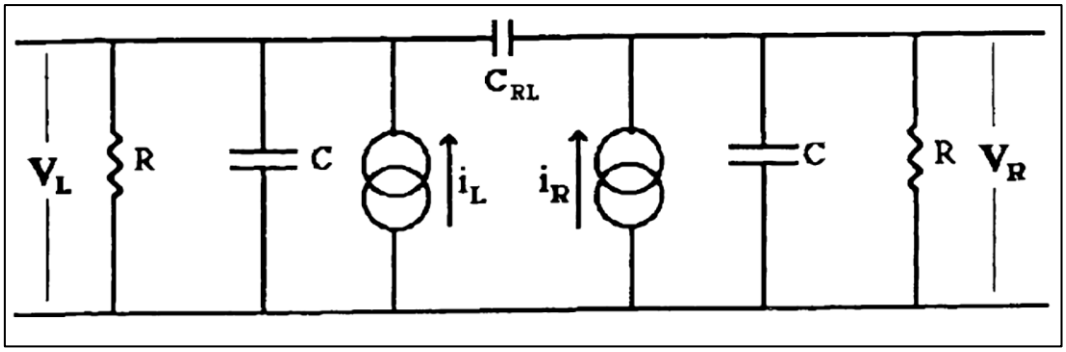

Figure 6: Equivalent circuit for an electrostatic pick-up. The signal sources are current generators with amplitudes specified in equation (16). Note that there is an inter-electrode coupling capacitance and a bleeder resistor is used to make the average voltage [17].

2.7. Linear response pickup electrode design

Consider a hollow tube with a radius b and length l inside a grounded beam pipe. If the tube is cut diagonally to make two electrodes as shown in Figure 7, the response to beam displacement is linear [17].

For example, a beam of charge density q_b is displaced by an amount r, θ from the axis of cylinder whose length is given by $l(\phi) = l(1 + cos\phi)$, the total charge on the inner surface of the cylinder is given as

$$Q_s = q_b l \int_0^{2\pi} \frac{(1+\cos\phi)(b^2 - r^2)}{b^2 + r^2 - 2br\cos(\phi - \theta)} d\phi \tag{18}$$

Upon integration, this becomes

$$Q_s = -q_b l\left(1 + \frac{\mathrm{r}\cos\theta}{b}\right) = -q_b l\left(1 + \frac{x}{b}\right) \tag{19}$$

Which is linear in beam displacement. The displacement sensitivity S_x then given by

$$\frac{R-L}{R+L} = S_x = \frac{x}{b} \tag{20}$$

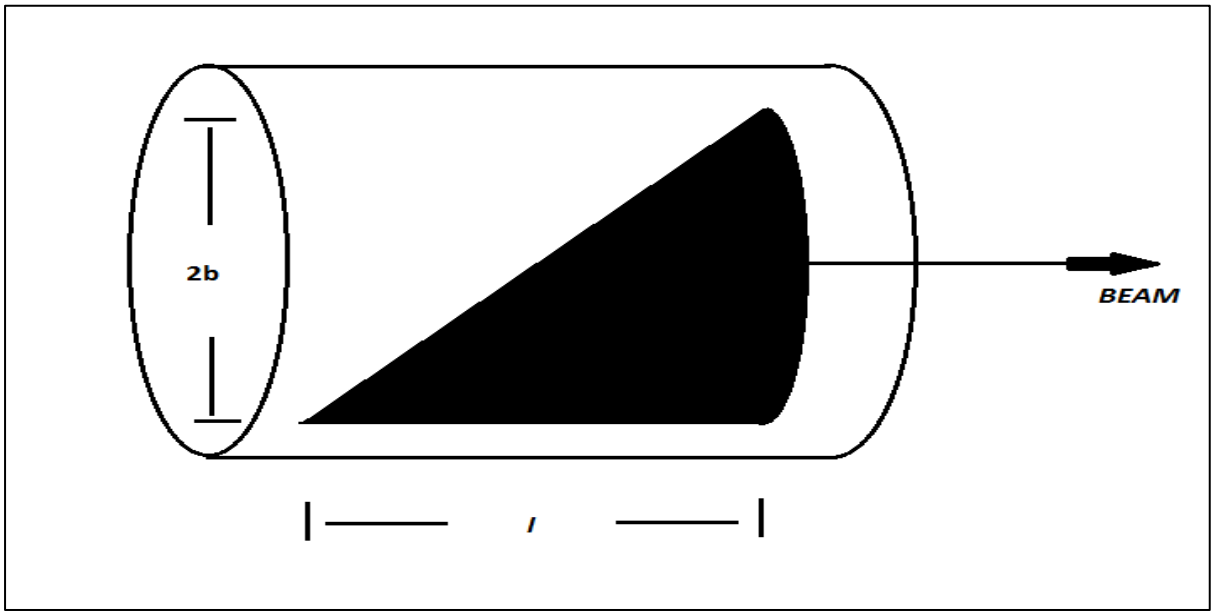

Figure 7: Side view of a diagonally cut cylindrical electrode that has a linear response to displace beams [12].

2.8. Beam Position Monitoring

The position monitoring of the charged particle beam can be achieved by coupling to the electromagnetic field of the beam. The idea is to measure the charges induced by the electric field of the beam particles on an insulated metal plate as shown in Figure 8. Since the bunched beam's electric field is time dependent, an alternating current (ac) signal is seen on the plate and coupled through radio-frequency technology [16].

For a continuous train of bunches, the frequency of the periodic beam bunches (and harmonics) is the carrier for the beam position information whereas for a single beam bunch, the derivative of the instantaneous beam current is the carrier [17]. The conventional beam position monitor is a pair of electrodes (or two pairs). The amplitude ratio of the induced signals gives information on the beam position at the beam bunching frequency or its harmonics. Since the position information of these signals is contained in the amplitude ratio, the information sometimes appears as AM (amplitude modulation) sidebands of the bunching frequency. In synchrotrons, the sidebands are displaced in frequency from the beam bunching signals [17].

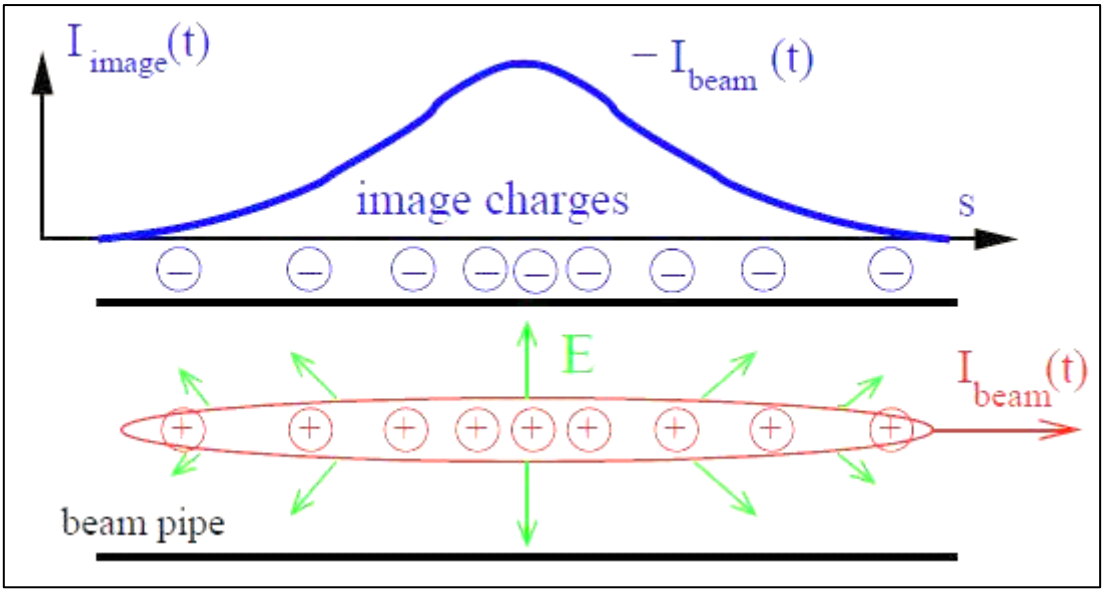

Figure 8: The beam current induces a image current of the same magnitude but reversed polarity in the beam pipe [16].

2.9. Signal treatment for capacitive pickups

General Formalism

In a capacitive pick-up, as shown in Figure 9, the induced image charge of the beam is coupled via an amplifier for signal processing. The plate at a distance b from the beam center has an area A and a length in longitudinal direction l. The current I_{im} [16] driven by the image charge Q_{im} is

$$I_{im} = \frac{dQ_{im}}{dt} = \frac{A}{2\pi bl} \times \frac{dQ_{beam}(t)}{dt} \tag{21}$$

For a beam with velocity βc, we can write the derivative of the beam charge $\frac{dQ_{beam}(t)}{dt}$

$$\frac{dQ_{beam}(t)}{dt} = \frac{l}{\beta c}\frac{dI_{beam}}{dt} = \frac{l}{\beta c} i\omega I_{beam}(\omega) \tag{22}$$

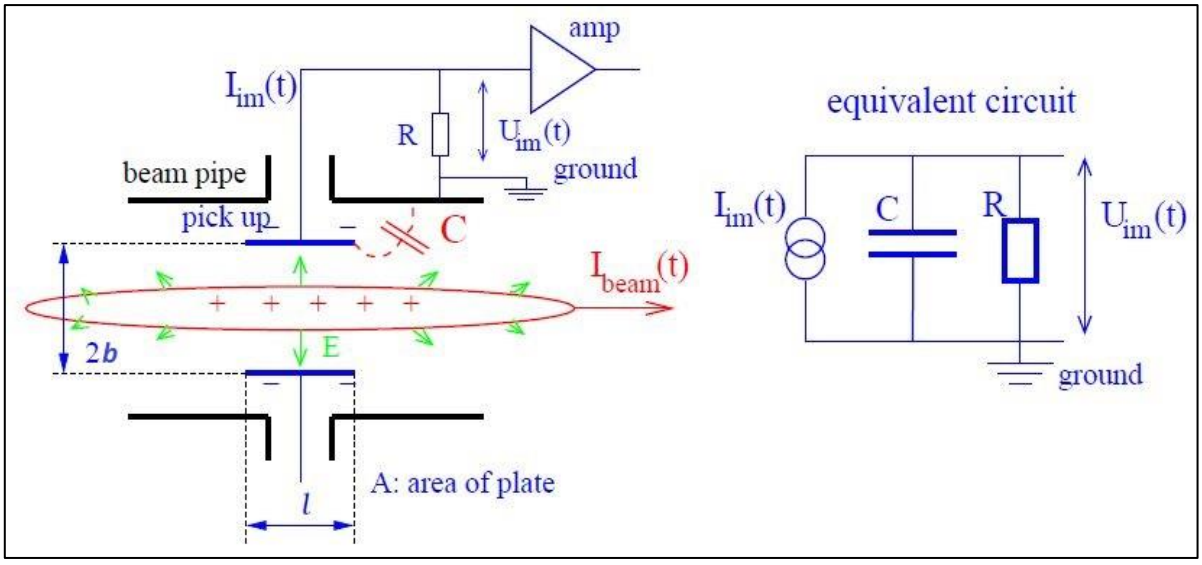

Figure 9: Circuit model of a pick-up electrode and its equivalent circuit for calculation [16].

where the beam current is expressed in the frequency domain as $I_{beam} = I_0 e^{-i\omega t}$. As the signal source uses the voltage drop at a resistor R

$$U_{im} = R \cdot I_{im}(\omega) = Z_t(\omega, \beta) I_{beam}(\omega) \tag{23}$$

For all types of pick-ups, the general quantity of longitudinal transfer impedance $Z_t(\omega, \beta)$ is defined in the frequency domain as per Ohm's law. It elaborates the effect of the beam on the pick-up voltage and its dependency on frequency, velocity and geometrical factors.

The capacitive pick-up has a certain capacitance C given by the distance with respect to the beam pipe and a capacitance contributed by the cable between the plate and the amplifier input. This amplifier has an input resistor R. Using a current source (image current) to model the beam and the parallel connection of the equivalent circuit, we can write the impedance Z as

$$\frac{1}{Z} = \frac{1}{R} + i\omega C \tag{24}$$

$$Z = \frac{R}{1 + i\omega RC} \tag{25}$$

Therefore the transfer function of the pickup is

$$U_{im} = \frac{R}{1 + i\omega RC} \cdot I_{im} = \frac{A}{\beta c C 2\pi b} \cdot \frac{i\omega RC}{1 + i\omega RC} = Z_t(\omega, \beta) I_{beam} \tag{26}$$

This represents a case of first order high pass filter with a cut-off frequency

$$f_{cut} = \frac{\omega_{cut}}{2\pi} = \frac{1}{2\pi RC} \tag{27}$$

For the linear-cut BPM case, the absolute value of the transfer impedance is

$$|Z_t| = \frac{A}{\beta c C 2\pi b} \frac{\frac{\omega}{\omega_{cut}}}{\sqrt{1 + \frac{\omega^2}{\omega_{cut}^2}}} \tag{28}$$

And the phase relation

$$\varphi = \arctan\left(\frac{\omega_{cut}}{\omega}\right) \tag{29}$$

A pick-up has to match the interesting frequency range, which is given by the acceleration frequency and bunch length. There are two different cases for the transfer impedance namely [16]:

High frequency range $f \gg f_{cut}$:

$$Z_t \propto \frac{i\frac{\omega}{\omega_{cut}}}{1 + i\frac{\omega}{\omega_{cut}}} \to 1 \tag{30}$$

The resulting voltage drop at R for this case is

$$U_{im}(t) = \frac{1}{\beta c C} \frac{A}{2\pi b} I_{beam}(t) \tag{31}$$

This shows that the pick-up signal is a direct image of the bunch time structure without phase shift i.e. φ≈0. Therefore, high impedance input resistors are used to get low frequency cut-off.

Low frequency range $f \ll f_{cut}$:

$$Z_t \propto \frac{i\frac{\omega}{\omega_{cut}}}{1 + i\frac{\omega}{\omega_{cut}}} \to i\frac{\omega}{\omega_{cut}} \tag{32}$$

Therefore the voltage across R in this case

$$U_{im}(t) = \frac{R}{\beta C} \cdot \frac{A}{2\pi b} \cdot i\omega I_{beam} = \frac{R}{\beta C} \cdot \frac{A}{2\pi b} \cdot \frac{dI_{beam}}{dt} \tag{33}$$

Using again the frequency domain relation $I_{beam} = I_0 e^{-i\omega t}$. From the equation, it can be seen that the measured voltage is proportional to the time derivative of the beam current. This can be realized by a high f_{cut} due to 50 Ω impedance. This 50 Ω termination is used to prevent reflections and to get smooth signal processing with a large bandwidth up to several GHz.

2.10. BPM position determination

Figure 10 represents the four electrode signals, where any of them can be represented by equation (26). And, implicitly in equation (26), their output voltage levels directly depend on the beam proximity to each electrode through the electrode current intensity, I_{img}, increasing as the induced current intensity of each electrode gets higher with a closer beam.

Thereby, the vertical and horizontal beam position variation will be detected by the two pairs of electrode outputs, $\{V_+, V_-\}$, and $\{H_+, H_-\}$, respectively, and the beam position coordinates will be determined by the difference between these output pairs, being: ΔV, the difference signal for the vertical plane, and ΔH, the difference signal for the horizontal plane. Moreover, in order to make the position measurement independent of the beam current, both Δ signals are normalized to the sum of all the electrode output signals, $\sum$, which is directly proportional to the beam current intensity. Then, the vertical and horizontal beam position coordinates will be given by

$$x_v \propto \frac{\Delta V}{\Sigma} = \frac{V_+ - V_-}{V_+ + V_-} \tag{34}$$

$$x_H \propto \frac{\Delta H}{\Sigma} = \frac{H_+ - H_-}{H_+ + H_-} \tag{35}$$

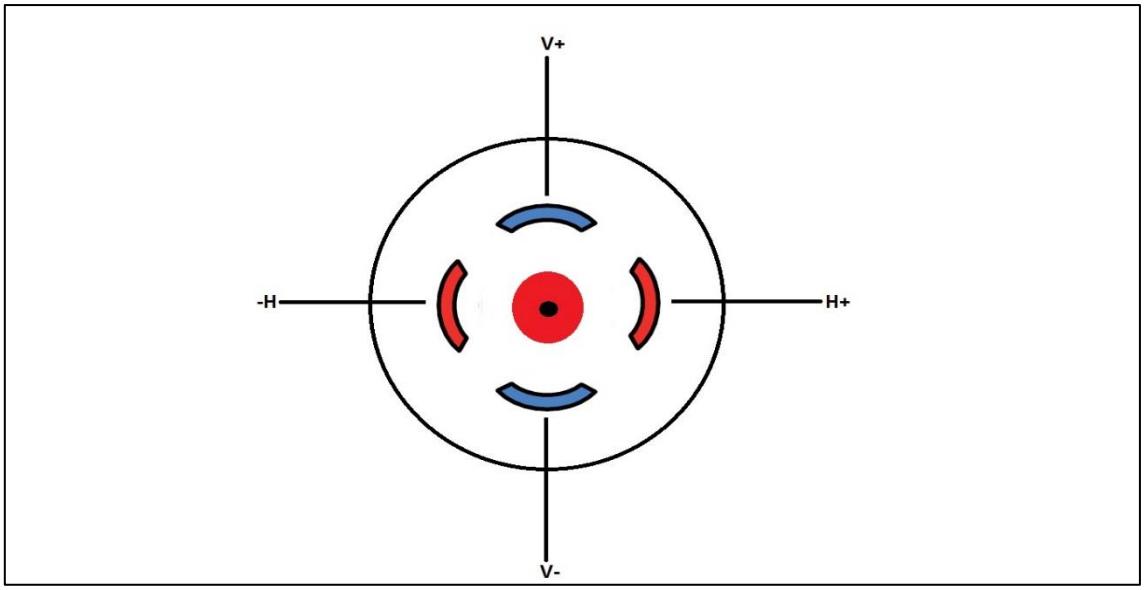

Figure 10: Capacitive pick-up schematic transversal view with signal outputs [18].

This method, commonly used for many pick-ups, for deriving the normalized beam position signal from the raw capacitive pick-up electrode signals, is called the difference-over-sum $(\Delta/\sum)$ processing. And the three $\Delta V, \Delta H \; and \sum$ signals will be obtained from a digitizer card connected to the capacitive pick-up outputs. As it was discussed in the previous subsection, the electrode output signals and, also, the Δ signals will show a good linear behavior for the beam position variation within the central region of the capacitive pick-up aperture. Therefore, a linear fit over sensitivity is used to characterize the capacitive pick-up and, thus, obtain the beam position coordinates from the presented signals. The linear relation to give the beam position coordinates from the Δ and $\sum$ voltage signals for the vertical (x_v) and horizontal (x_H) planes are

$$x_V = EOS_V + K_V\left(\frac{\Delta V}{\Sigma}\right) \tag{36}$$

$$x_H = EOS_H + K_H\left(\frac{\Delta H}{\Sigma}\right) \tag{37}$$

where $K_{V,H}$ are the characteristic slopes which depend on the capacitive pick-up sensitivity to the beam position changes in each plane, and $EOS_{V,H}$ are the Electrical Off-Sets from the capacitive pick-up's mechanical center for both coordinates. Like the electrical off-sets, the capacitive pick-up's sensitivity for each coordinate plane are important characterization parameters and from equation (36) and (37), they are defined as $S_{V,H} \equiv 1/K_{V,H}$. The sensitivity for each coordinate plane, $S_{V,H}$ gives

the variation of ΔV or ΔH signals (since $\sum$ is a constant normalization parameter) when the beam changes its position in the vertical or horizontal directions.

Usually in the capacitive pick-up characterization tests, the position is known and the $\Delta/\sum$ parameters for both planes are obtained. Therefore, the sensitivity parameters are obtained from the inverted linear fit equations or characterization equations shown below

$$\left(\frac{\Delta V}{\Sigma}\right) = n_V + S_V x_V \tag{38}$$

$$\left(\frac{\Delta H}{\Sigma}\right) = n_H + S_H x_H \tag{39}$$

Where $x_{V,H}$ are the positions, and $n_{V,H}$ are the $\Delta/\sum$ parameters deviation when the beam is in the center, which are directly related to the electric off-sets defined in equation (36) and (37). One has to take into account that the sensitivity is defined as a characteristic parameter of the capacitive pick-up, so the Δ and $\sum$ signals must have the same gain factor to get the true sensitivity of the capacitive pick-up, or if it is not the case, the measured sensitivity must be divided by the $\Delta/\sum$ gain ratio.

The overall precision/accuracy with which the beam position can be determined is limited by aggregation of mechanical alignment errors, mechanical tolerances in the capacitive pick-ups, calibration error in the electronics, attenuation and reflections in the connecting cables, electromagnetic interference and circuit noise. All these will reflect in the positional error which are deviations from the ideal capacitive pick-up's linear behavior. An error analysis can be performed from equations (36) and (37) to yield the linearity errors of each position with a standard deviation, σ, to represent the uncertainty in absolute beam position measurement. The overall precision/accuracy is calculated as the rms of all position errors in the beam position range of interest for the vertical and horizontal planes, respectively [18].

2.11. Electronics for signal processing

General Considerations

The electronics circuits connected to the BPM electrodes influence the properties of the signal shape and is therefore important for the complete installation. In modern installations, the analog signal from the electrodes is digitized early in the signal chain and digital signal processing provides the position information, flexible signal evaluation without any hardware changes [16]. The required signal processing is realized on a Field Programmable Gate Array (FPGA) for ensuring fast, real-time response. Figure 11 represents scheme of an electronics board designed for use at the HESR for setup.

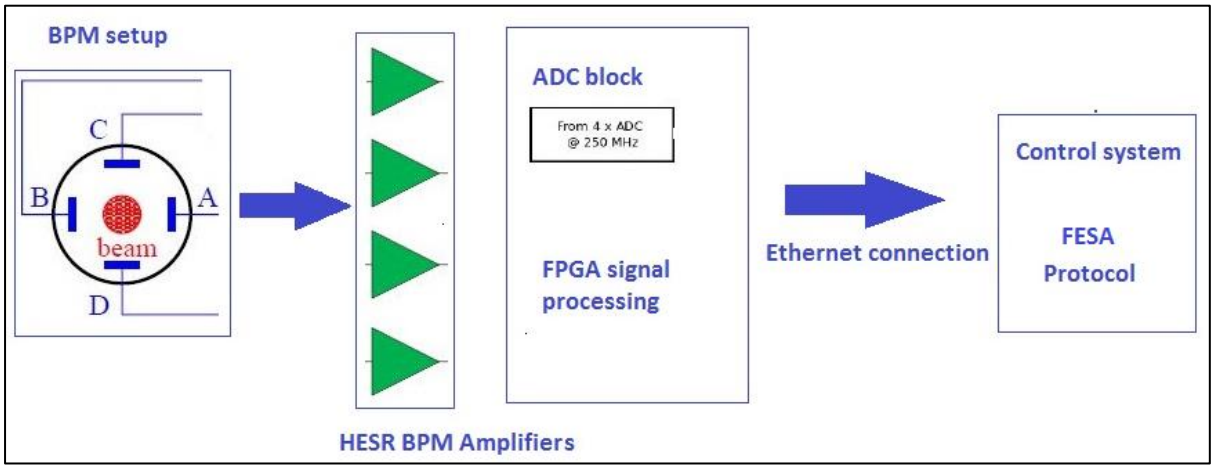

Figure 11: Scheme of digital BPM electronics readout for the HESR BPMs [19]. Signals from the BPM electrodes can be recorded at the control system via Ethernet using FESA protocol. The signal processing works on a FPGA platform which receives raw ADC data from the HESR BPM amplifiers.

Raw pickup signals A, B, C and D are amplified using HESR BPM amplifiers and enter the processor module. Here it is processed, stored and formatted along the way before being sent to the control system. The processing consists of analog signal processing, sampling, digital signal processing and position calculation [19]. As standard processing unit for the BPMs within the FAIR project, the commercially available product "Libera Hadron" from Instrumentation Technologies d.d. was chosen. Some of the Basic parameters and target performance of the Libera Hadron is shown in Table 2.

Sl.No	Parameters	Description/Values
1	Number of electrode RF inputs	4
2	Input signal	Bipolar/Unipolar pulse trains at repetition rate frequency
3	Input impedance and connector type	>50 Ω SMA
4	Pulse maximum voltage	±1.25 V peak
5	Main sampling frequency	250 MHz
6	ADC Resolution	16 Bit
7	Typical bunch-by-bunch uncertainty, U_{in} = 1.5 V peak, pulse FWHM = 100 ns	≈4 µm

Table 2: Basic parameters and target performance of the Libera Hadron electronics [19].

HESR BPM amplifiers

The amplifier signal will handle signals coming from the capacitive BPMs. Depending on various beam intensities, adaptation to signal level is crucial. This will be achieved using non-inverting, low-noise amplifier quartets. The fundamental requirement of these quartets is common mode amplification behavior. Attestation of this behavior is foreseen with internal test generator signals for every gain range. An additional calibration input and monitor outputs are under construction for external network analyzer. This is to check the gain factors precisely. Another important necessity is the dose consideration of the quartets i.e. 1000 Gy for 2 years as they will be operated in a radiation environment [20]. The basic parameter list of these amplifier quartets can be found in Table 3.

Sl.No	Parameters	Values
1	Input impedance	50 Ω
2	Input VSWR	≤1.2
3	Input Source capacitance	1 nF
4	Output level	±2V peak
5	Output impedance	50 Ω
6	Output VSWR	≤1.2
7	Output load capacitance	10 nF (max)
8	Gain ranges	-50 dB to 60 dB

Table 3: Basic parameters of the HESR BPM amplifier that will be used in the actual installation [20].

3. Design background of BPM prototype and wire test bench

3.1. Design of the HESR BPM prototype

Capacitive pickups are under manufacturing for closed-orbit measurements at the FAIR. These BPMs should be able to measure approximately 10^8 to 10^{11} particles and provide adequate information about beam trajectory.

As explained in the previous chapter, diagonal cut capacitive pickup is a device of choice for beam diagnostics in hadron machines due to its high linear response and large sensitivity [17]. In order to determine the position of the beam, the signals generated at each electrode is compared to one another. Moreover, to avoid impedance mismatch in the vicinity of monitor edges, the inner diameter of the cylindrical pickup is the same as that of the straight section of the beam/vacuum pipe of the HESR. The beam pipe that houses the BPM is shown in Figure 12.

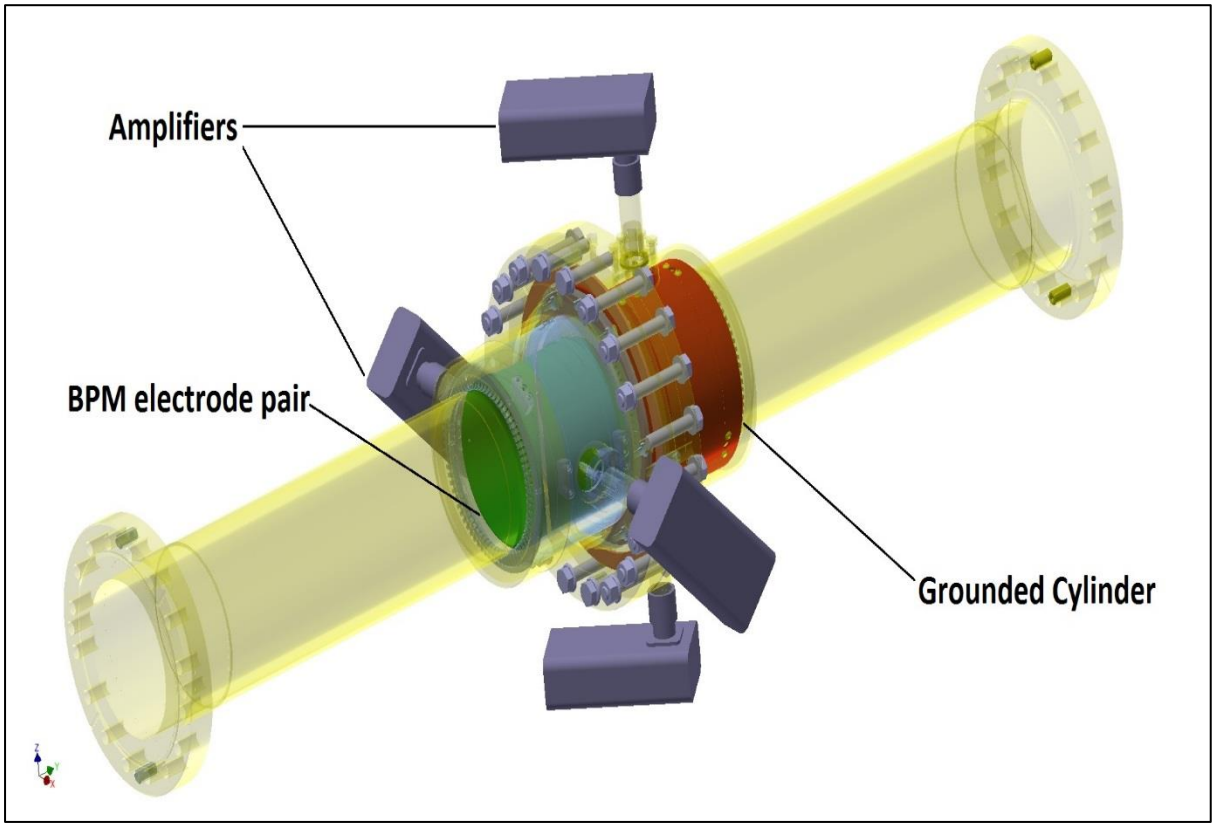

Figure 12: Beam pipe housing the BPM electrode pairs and grounded cylinders.

The design parameters and requirements for the BPM prototype are shown in the Table 4.

Parameter	Symbol	Value
Duct radius	b	56 mm
BPM electrode pair length	L	77 mm
Linear cut gap(Diagonal Plane)	d	3 mm
Subtended angle of linear cut	θ	55.5 degrees
BPM Electrode radius	a	44.5 mm
HESR revolution frequency	B	500 kHz
Overall Accuracy of closed orbit measurement for 10^{10} antiprotons including processing electronics	$\upsilon_{V,H}$	≤ 100 µm

Table 4: BPM design parameters and requirements.

The design of the HESR BPM has been selected according to the COSY BPM which itself is adopted from CERN. It is a capacitive pickup with current designation: "Linear-cut BPM in cylindrical geometry". They are characterized by their linear response as explained in section 2.7. The electrodes are held in place by a grounded hollow supporting cylinder (galvanically isolated). The BPM electrode is as shown in Figure 13.

This arrangement results in a capacitive coupling. This capacitive coupling allows the electric influence of a charged particle beam, whereby the mirror current becomes larger with the beam current that flows to the electrode in the opposite direction. In this way, the mirror current is replaced by the waveform of the time derivative of the beam current.

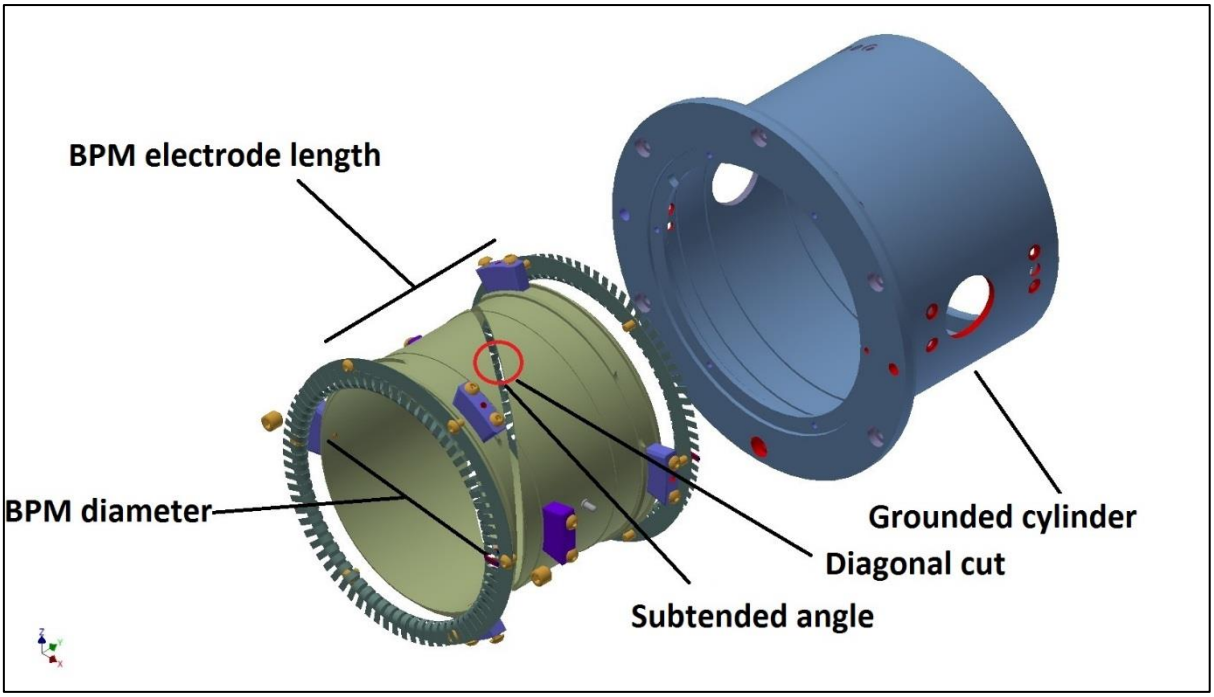

Figure 13: BPM electrode pair with grounded cylinder.

As the beam bunches are much longer than the BPM, the electric field propagation in the BPM can be approximated with a Gaussian wave traveling on a wire. The effects of non-relativistic beams is minor and can be neglected. This is achieved experimentally by stretched wire method. The amplitude change of the signals induced in the electrode is measured as a response on the changing wire position.

3.2. Scope of the work: Design of the stretched wire test bench

Prior to beam operation, it is necessary to characterize the BPM which involves: establishing a relationship between beam position and sensitivity and determining its electrical center. This will be achieved with the help of a standalone test bench using the stretched wire method. Therefore, a test bench is designed and constructed to calibrate the BPM. Followed by which, is the development of a software/application which can perform automated tests.

3.2.1. Stretched wire test bench

A test bench is a virtual environment with tools for measurement and manipulation to manually verify the correctness of a device under test (DUT), here, beam position monitors (BPMs). The test bench that will characterize the BPMs for the HESR will be stimulus type, containing a stimulus driver and the DUT. This will eventually provide a conditioned response elicited by the stimulus.

The fundamental design concept is the in-tower mounting of the BPM along with its main stand elements within two BPM reference boxes (explained later) made of structural steel and aluminum sheets. Such a design is preferred in order to accommodate BPM assembly of varying lengths for characterization tests. This also aids in realization of the stretched wire passing through the hollow center of the BPM, thus avoiding any wire bending due to gravity. The whole setup is rested on a granite slab of surface flatness in sub-micrometer range in order to maintain the orthogonality of the stretched wire with respect to the beam pipe's cross section. Moreover, the granite slab helps to slide the reference boxes on their reference edges to precisely mount the BPM and also to damp the ground vibrations.

With the BPM fixed on the BPM reference box from either ends, the stretched wire is moved by linear stages to yield wire-BPM relative displacement through their position readout. Moving the wire instead of the BPM is preferred as the calculated weight of the BPM assembly exceeds the normal load capacity of the linear stages. Figure 14 represents the design sketch of the test bench setup with its working components.

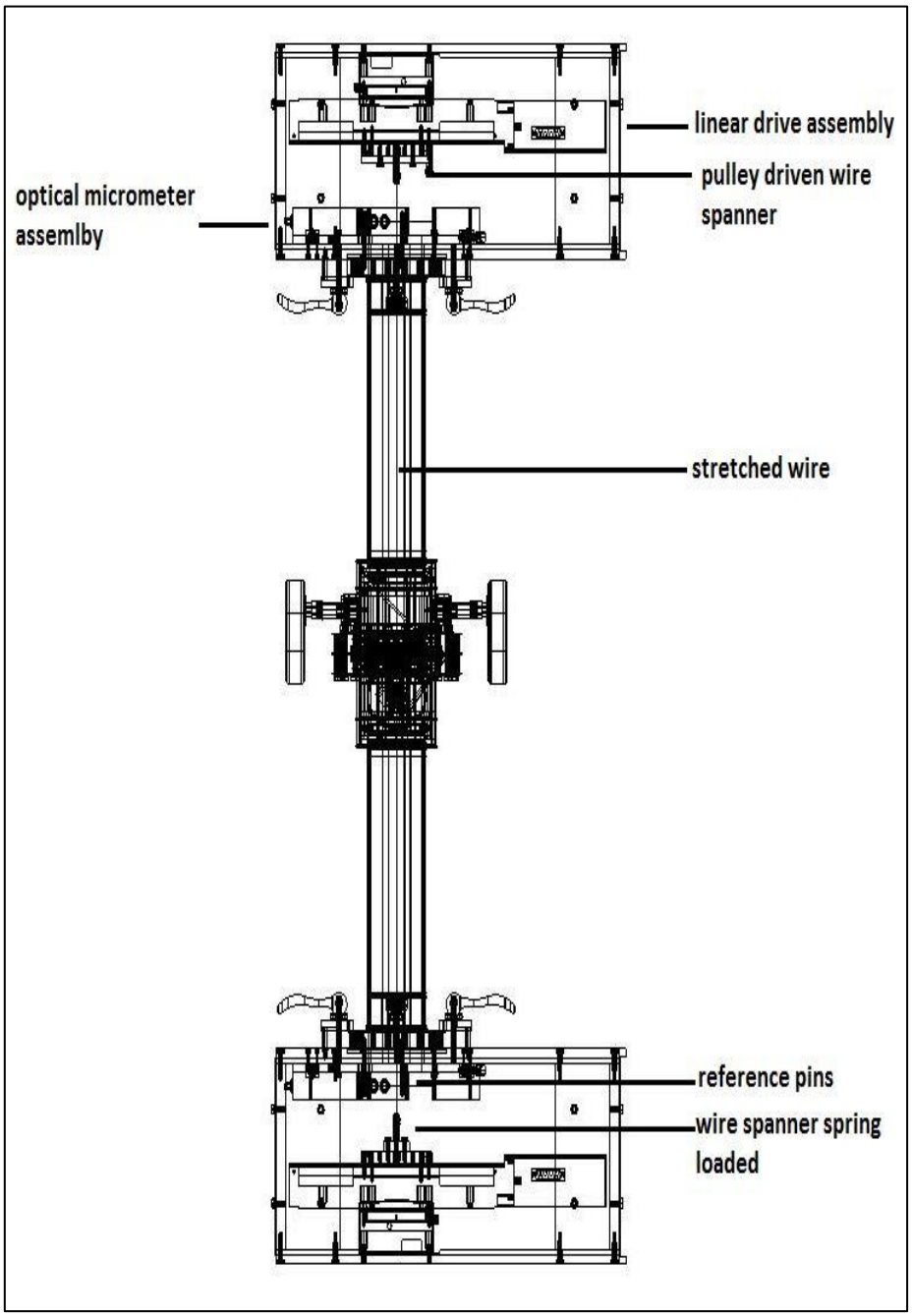

Figure 14: Design of test bench with its working components.

The working components of the test bench are the following:

a) BPM and its assembly: Figure 13 shows the 3D view of the HESR pickup electrodes. The prototype BPM assembly, Figure 15, housing the grounded cylinder at its center, has its both ends fixed with a non-rotatable flange. Moreover, the vacuum surface on these flanges house two reference pins made of ceramic (each on X and Y plane) at 10° offset in clockwise direction, at a radius of 50.5 mm. The material for the reference pin is chosen as ceramic in order to prevent diffusion bonding of it with the beam pipe's flanges.

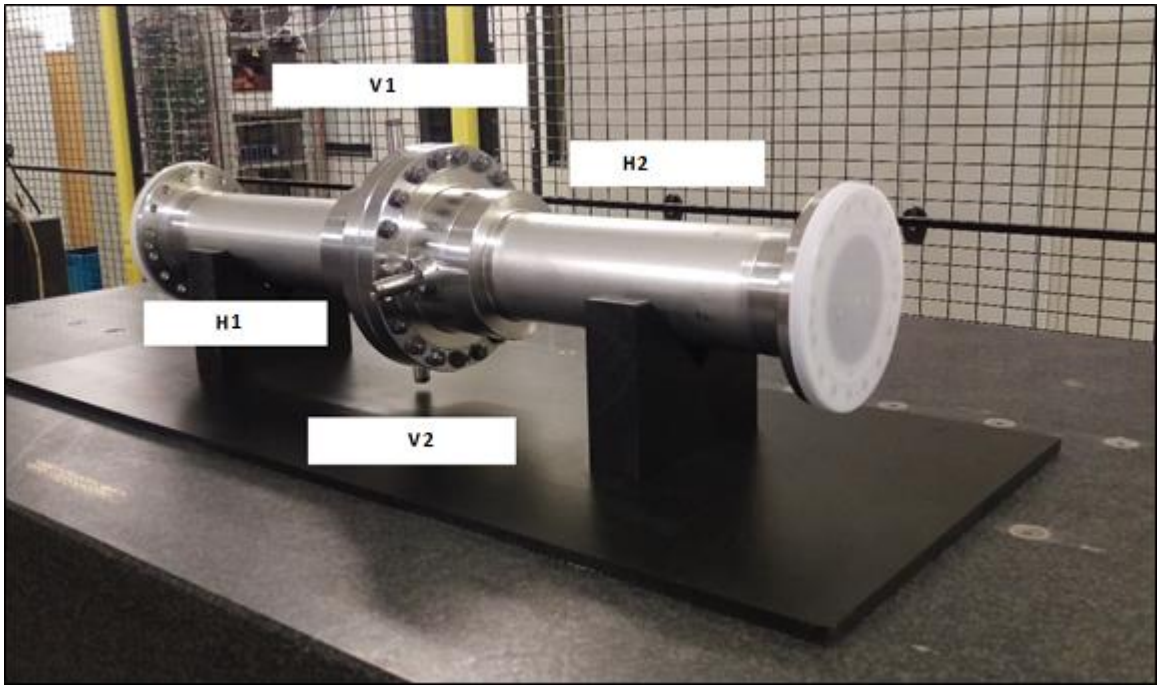

Figure 15: Beam pipe with BPM assembly at its center and its electrode position markers.

b) BPM reference box: Two reference boxes (same dimensions) made of structural steel is mounted to the BPM from either ends. The reference box, as shown in Figure 16, is provided with precisely machined reference edges (marked). The reference pins, guides through precisely reamed holes provided on the upper surface (marked) of the reference box. Such a strategy is chosen for the assembly, primarily to minimize mechanical offsets while mounting and also to zero the mechanical aberrations on the vacuum surface. The reference box also entails press clamps (in red) to secure the BPM assembly.

c) Optical Micrometers: Two RF656-25 optical micrometers [21], from Riftek Ltd., is mounted in XY assembly, as shown in Figure 17, from the inside of the upper plate of the BPM reference box. The two reference pins, mentioned earlier, fall within the micrometer's measurement range, as represented in

Figure 18. Such an arrangement is preferred, as the homing position of the beam analogue i.e. the stretched wire will be preset with respect to these reference pins.

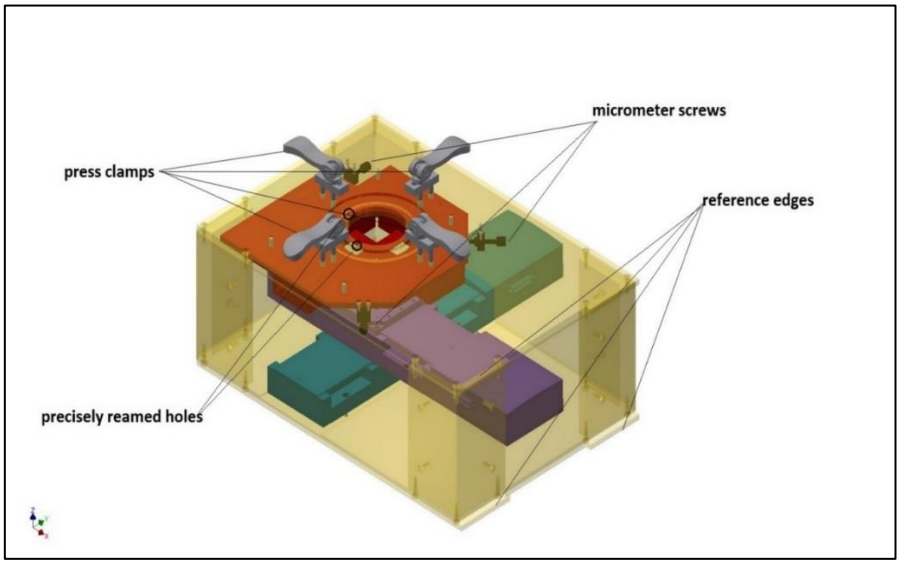

Figure 16: BPM reference box. Inside the box are two 90° mounted linear drives that move the wire, simulating the ion beam. The position can be verified with 2 optical micromters. Using the press-clamps, the BPM mounted inside a vacuum pipe can be attached to the box. 2 boxes are necessary to perform the test.

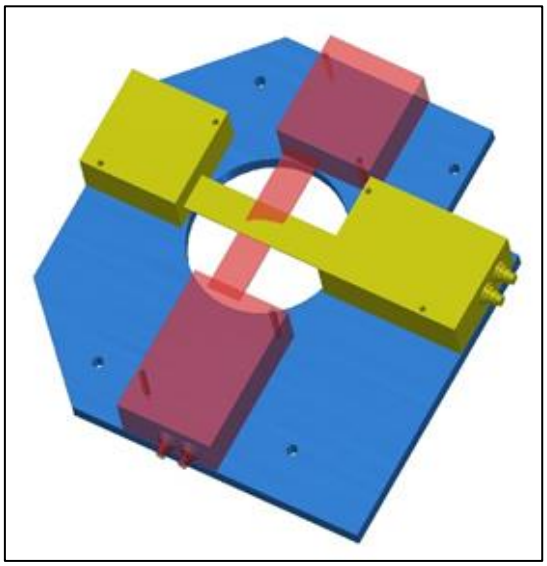

Figure 17: XY assembly optical micrometer. The area covered by the micrometer is only a fraction of the possible moving range of the wire. Therefore, outside the covered area of the optical micrometers, the reference from the linear drives, moving the wire is solely used.

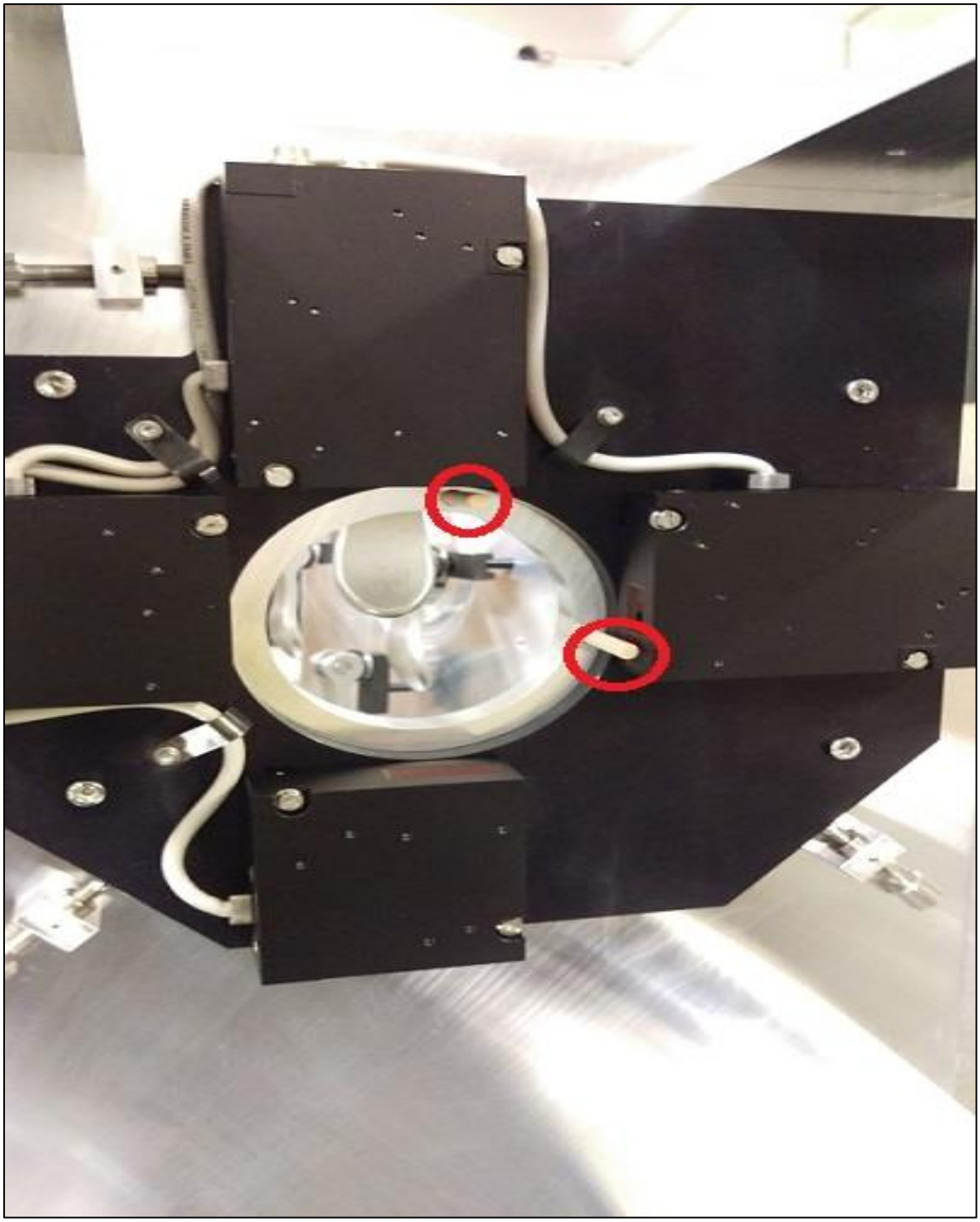

Figure 18: Optical micrometer assembly with reference pins marked in red. These reference pins have an absolute reference to the BPM when mounted to the test stand. The pins are located such that they are within the coverage area of the optical micrometers.

d) Linear stages: The two linear stages are orthogonally mounted (as master-slave i.e. XY assembly) on the base plate of the BPM reference box, providing the wire-BPM relative displacement in (X, Y) direction. The M- ILS150HA, shown

in Figure 20 as XY assembly, was chosen for each linear stage, being a high performance precision linear system driven by DC motors from Newport Corporation [22]. The maximum linear travel range is 150 mm with an on-axis accuracy of ±2 μm and the smallest incremental linear motion of 0.3 μm. The maximum normal load capacity is 250 N (25.5 kg) which can withstand the weight considerations of the wire elements in the test bench.

e) **Wire Elements:** Copper wire of 0.4 mm is stretched through the BPM assembly, from the upper BPM reference box to the bottom BPM reference box. This is achieved by fixing it between the wire spanners and allowing it to pass through the BPM assembly, thereby using one of the spanners as a hanging weight, thus employing gravity. In the bottom BPM reference box, the wire spanner is mounted on a spring load to compensate for tension variation whereas in the upper BPM reference box, the wire spanner is mounted on the pulley platform to provide easy access and also to stretch the wire.

f) **RF matching networks:** The RF matching networks is used to provide undisturbed excitation signal and also to minimize reflections. This is of importance for frequency response tests and is achieved through impedance matching. Two resistors of 273 Ω and 323 Ω are connected in series to the wire at the lower and upper reference boxes to achieve impedance matching as shown in Figure 19.

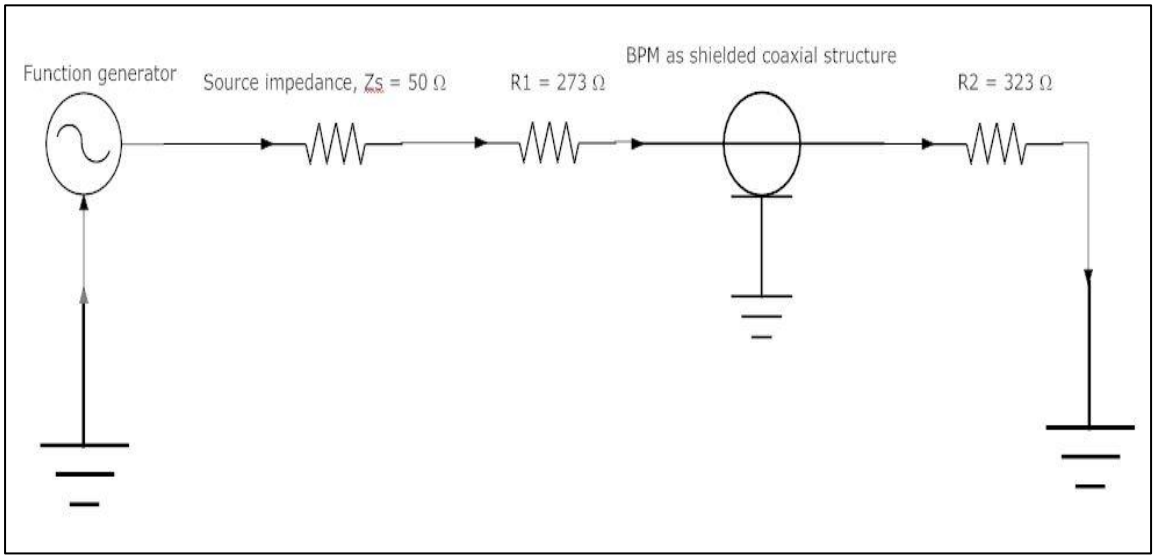

Figure 19: Impedance matching network to minimize reflections and maximize transmission.

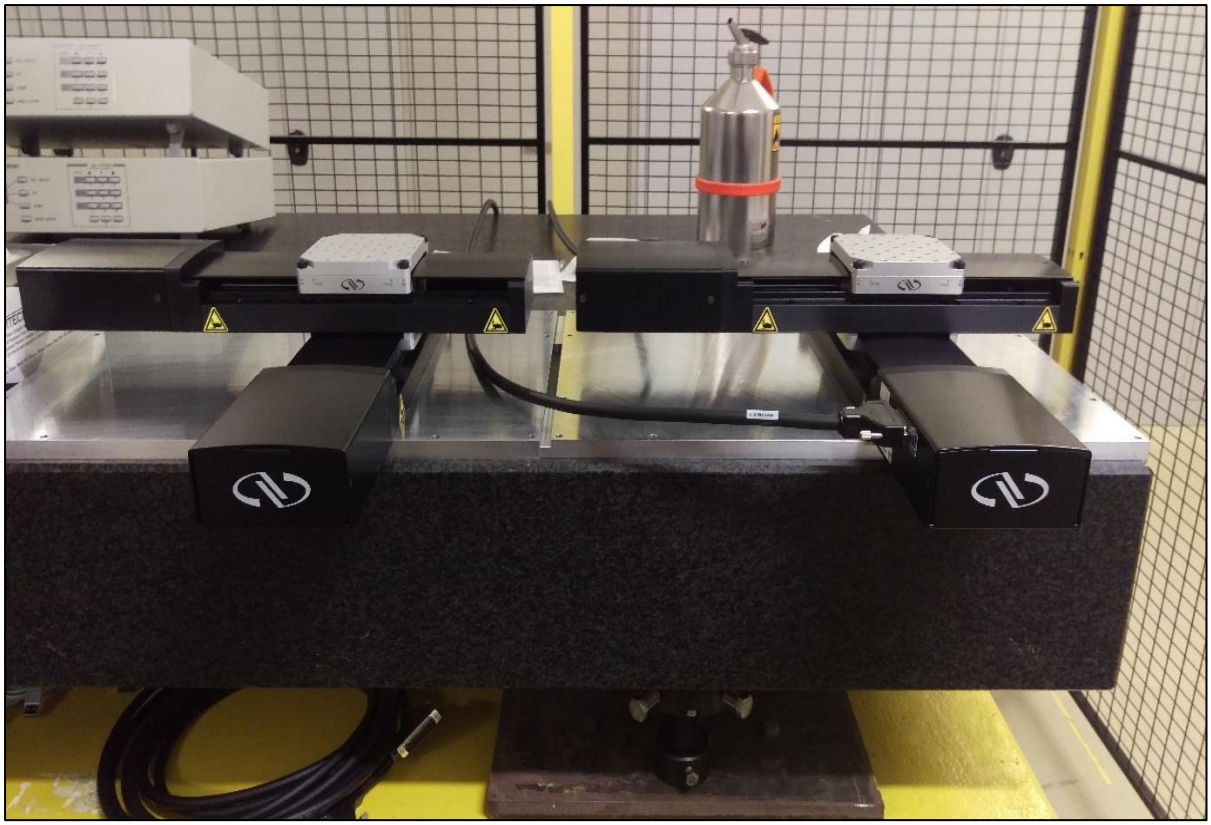

Figure 20: XY assembly of linear drives from Newport mounted on base plates of both the reference boxes.

3.2.2. Metrology Inspection of the test bench components

Based on BPM requirements, for the design of the test bench, we have decided a target accuracy of 50 µm in positional measurement of the BPM. Therefore, the uncertainties that can be introduced by the test bench should be minimized, as it is required for linearity and offset characterization tests. This is critical for such high precision measurements as the misalignments of the wire in the test bench can adversely affect the accuracy of the HESR BPMs. In such sense, the typical misalignments that were considered in this metrology test includes mechanical fabrication, positional uncertainties of linear drives and optical micrometers and the assembly of the test bench elements. These uncertainties were minimized while assembling the test bench components with the help of a 3D Coordinate Measuring Machine (CMM) in ZEA. Moreover, the concerns that the test bench could be deformed under load conditions was eased by Finite Element Analysis stress analysis simulation, giving maximum displacement in nanometer ranges, as shown in Figure 21.

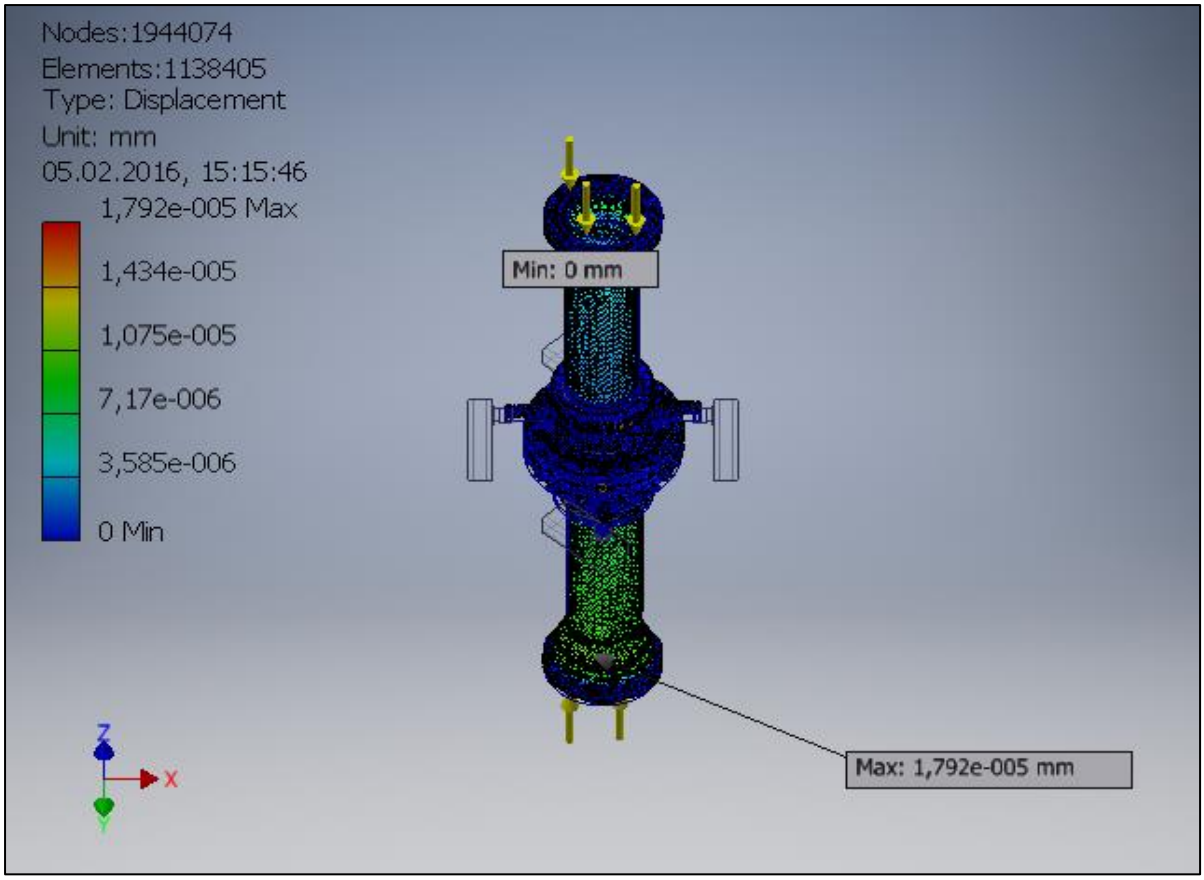

Figure 21: Finite Element Analysis (FEA) of the BPM prototype under load conditions twice of the actual situation. This was perfomed using Autodesk Inventor.

However, there is a possibility to have misalignments of the functional components of the test bench with use. This is eradicated by having online metrological inspections which can be classified as the following:

a) Wire tilt correction: The inclination of the wire with respect to the BPM cross-sectional plane is measured by the XY assembly of optical micrometers RF656-25 on either ends of the BPM assembly. Deviations in the positional information from the micrometers imply wire tilt. This is rectified by correcting the positions of the linear drives until same measurements are observed in micrometer assemblies. But the prerequisite for this inspection is to position the optical micrometer assembly coaxially with respect to the BPM cross section such that the positional readout from the optical micrometers is the same for all the reference pins. Figure 22 represents a conceptual sketch of wire tilt correction.

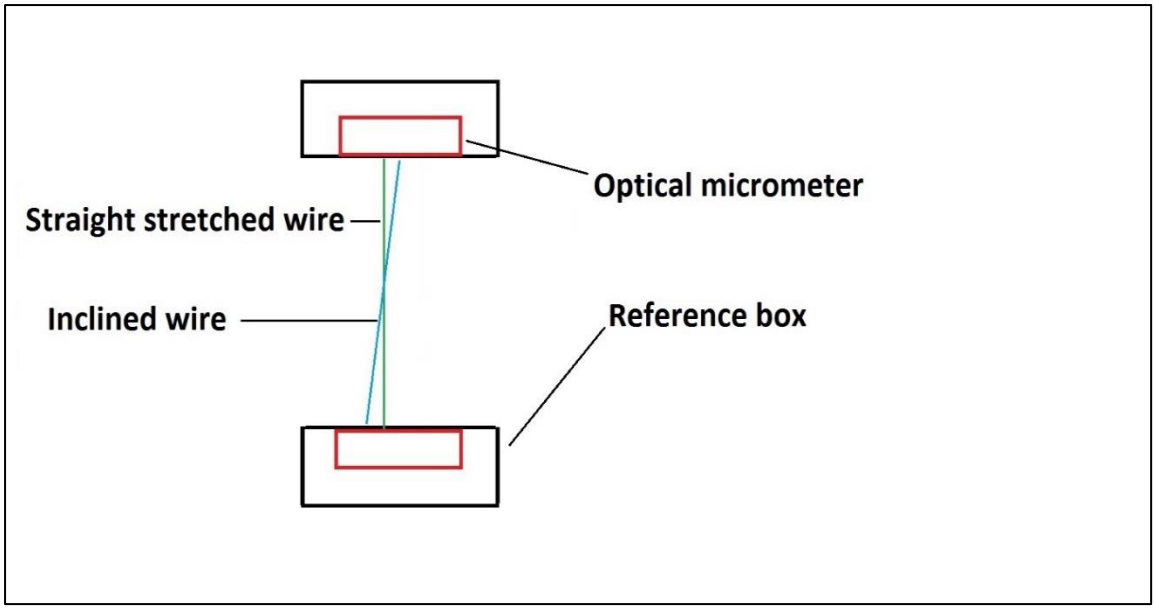

Figure 22: Block diagram of wire tilt correction.

b) Coplanar linear drive and micrometer assembly: The coplanar arrangement of the linear drive assembly and the micrometer assembly aids in reducing positional uncertainties. Such uncertainties are rectified by the usage of micrometer screws on the optical micrometer platform after comparing optical micrometer readings of the reference pins with the reading from ZEA. Figure 23 represents such an assembly achieved with the help of the 3D CMM from ZEA inspection department.

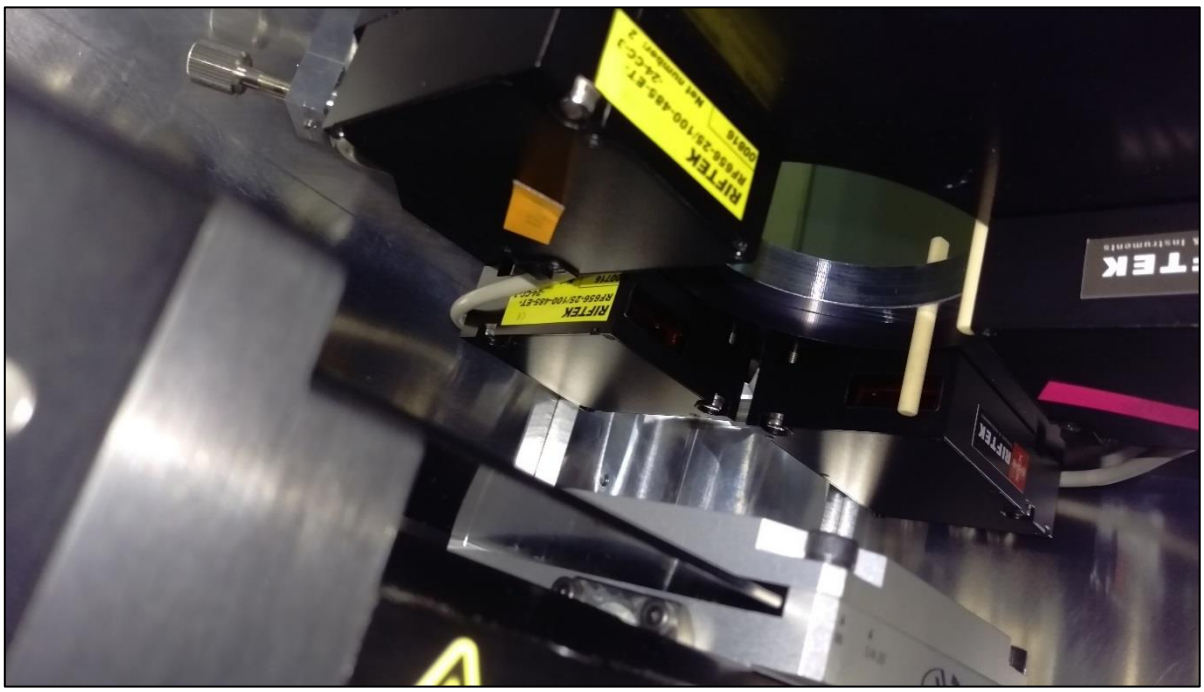

Figure 23: Coplanar linear drive and optical micrometer assembly.

c) **Wire offset correction:** Followed by the wire tilt correction, the wire is positioned at the BPM mechanical center with the help of linear drives. The optical micrometer platform is placed coaxially, as such an arrangement would mean on-plane observation of the BPM cross-section. After positioning the wire at the BPM mechanical center with the linear drives and verifying with optical micrometers, this position is referenced as the home position for further measurements.

In this test bench, the uncertainties due to wire rotation on the wire center is minimized as the arrangement of the test bench restricts these. This is determined by the readings of the linear drives provided the optical micrometer reading remains unchanged in the cross-sectional plane. This is an important parameter as by definition the wire center is the only point which does not change its position under rotation or torsion. Figure 24 represents a sketch of wire offset correction.

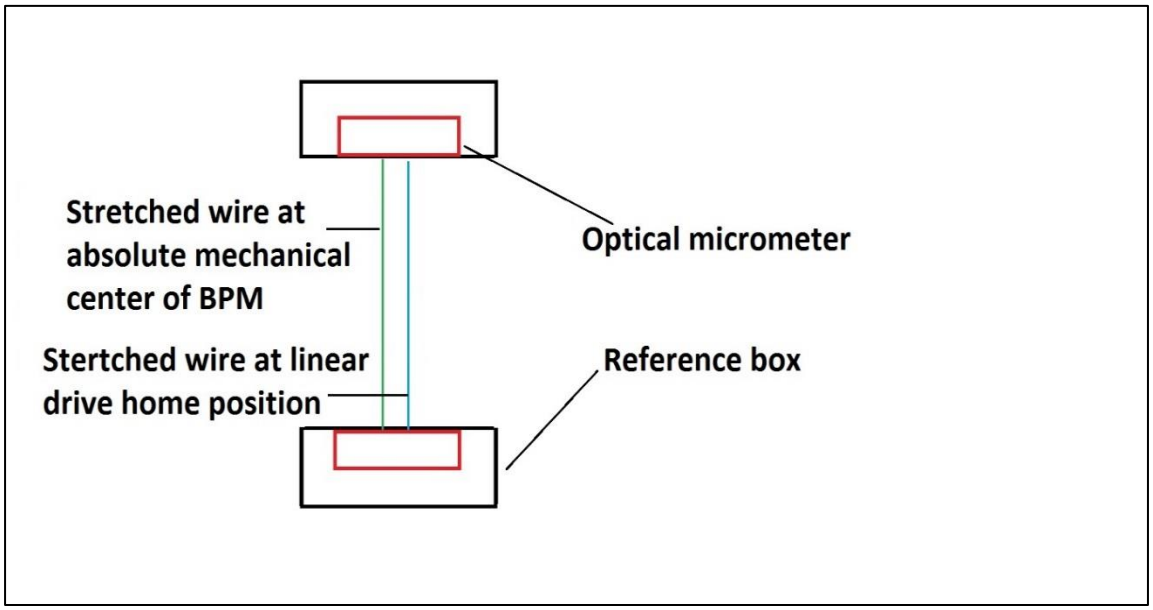

Figure 24: Wire offset correction.

d) **Orthogonalism and parallelism of wire trajectories:** The relative orthogonality between the linear drives mounted in XY configuration is 0.029° which was achieved with the help of ZEA. The theoretical change in the trajectory followed by the wire does not vary beyond 0.8 µm. Nevertheless, the wire trajectory deviation will be measured with the help of optical micrometers on either ends for a wire travel within the optical micrometer's measurement range, obtaining much smaller deviations. The pitch and yaw of

the linear drive is ±75 µrad (±0.0043°) and ±50 µrad (±0.0029°). Corresponding to these deviations, (pitch is responsible for non-parallelism), the slope of the X and Y coordinate is 0.0875 µm/mm. Hence, for a linear travel of 10 mm in either X or Y coordinate, will result in a deviation (both ends) of 0.875 µm.

4. Characterization tests of the BPM prototype

Characterization tests at low frequencies were performed on the BPM prototype at 500 kHz as this is the operating frequency of HESR. In order to employ the BPM, linearity tests for positions in the range of interest were performed. This helps to measure the BPM working parameters, sensitivity, and electrical offsets in horizontal and vertical planes independently. To fulfill the performance specifications of the HESR BPMs, the accuracy and resolution benchmarks of the BPM position measurement are determined from the linearity test [18]. These low frequency characterization tests were realized with the stretched wire test bench setup explained in the previous chapter. The test bench imitates the beam passing through the BPM by a thin stretched conducting wire (diameter of 0.4 mm) which carries a given AC current and can be translated to multiple positions with the help of linear drives relative to the BPM vacuum pipe aperture. Inherently, the conducting wire forms a coaxial cable structure with a characteristic impedance of 323 Ω with the vacuum pipe of the BPM and can reproduce a pencil beam behavior. This is possible only when both have the same transverse electric and magnetic fields propagating down the vacuum pipe and generates a purely transverse wall image current mirroring the stretched wire.

4.1. Raw capacitance measurement

Before performing linearity characterization tests, it is necessary to confirm electrically the design of the BPM prototype. This was confirmed by measuring electrode raw capacitances with the help of a universal LCR meter as shown in Table 5. The LCR meter has 1% error in measurement and even with this error, the values are identical within the error margins.

Sl.No	Electrode	Capacitance in pF
1	H1	30.9
2	H2	30.7
3	V1	30.7
4	V2	31

Table 5: LCR meter measurements of individual electrodes in the prototype BPM.

4.2. Instrumentation equipment setup

Figure 25 represents the block diagram of the instrumentation equipment setup for BPM linearity characterization test of the stretched wire test bench with all the associated instruments, connection schemes and involved signals. Figure 26 shows the complete setup that was assembled.

The instrumentation setup was envisaged with the objective of automatizing the motion control of linear drives, and measurements (data readout) from the BPM prototype. This process not only increases the reliability of the test measurements but also increases the reproducibility.

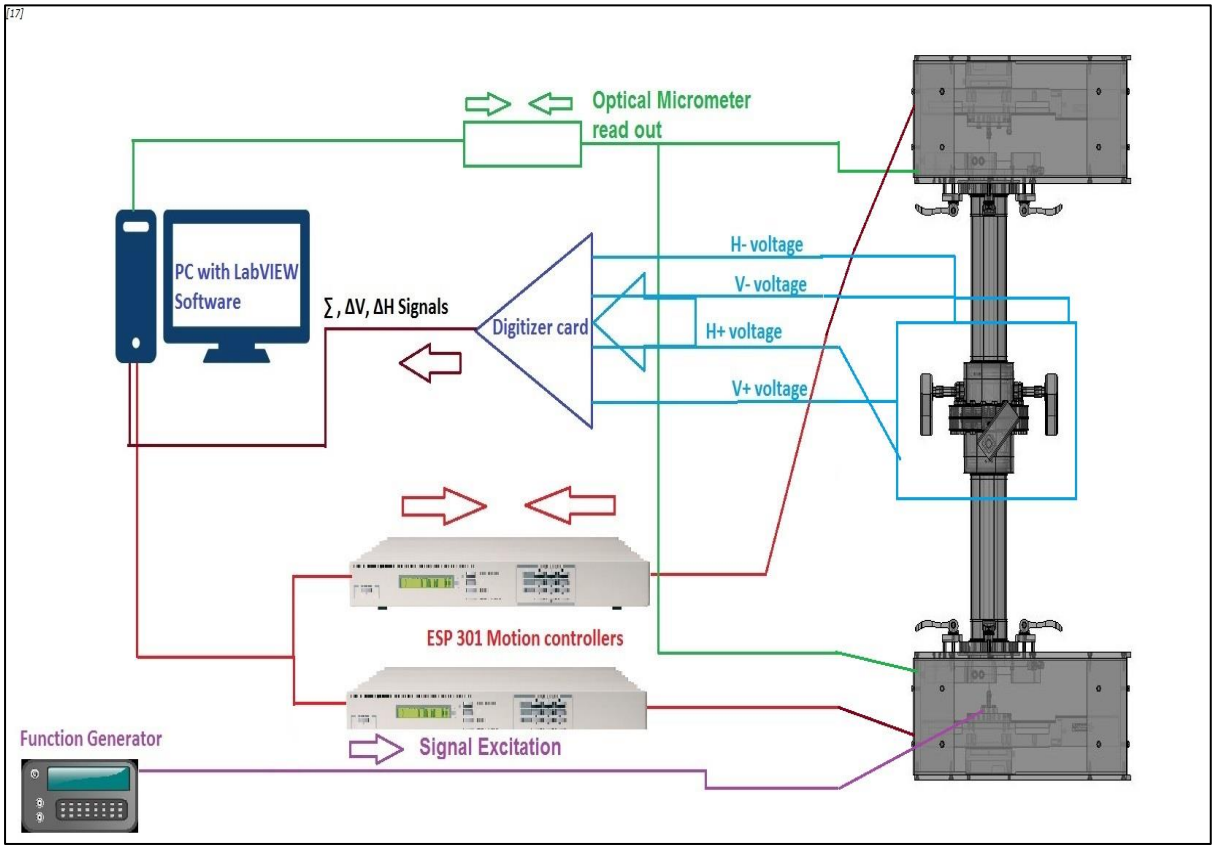

Figure 25: Block diagram of the instrumentation equipment setup and test bench. Wire is excited with a Gaussian signal through a function generator. The electrode signals are read through a digitizer card by a LabVIEW application.

The key element in the instrumentation setup is a PC running a LabVIEW software/application for the control and data acquisition of the whole test setup. The PC is equipped with a Spectrum Systementwicklung Microelectronic GmbH M4i.4421-x 16-bit, 250 MHz sampling rate ADC digitizer card to process signals.

This was used as at the time of tests, the foreseen readout electronic "Libera Hadron" was not available. However, the digitizing parameters of both Spectrum and Libera are profoundly similar.

A LabVIEW application calculates the horizontal $\Delta H/\sum$ and vertical $\Delta V/\sum$ voltage amplitudes corresponding to each programmed wire position. Both results are directly saved to the PC for further processing of linearity test data. This application is also responsible for the linear stages control through ESP 301 motion controllers from Newport Corporation [23], and the optical micrometer positional streaming except the control of the signal generator.

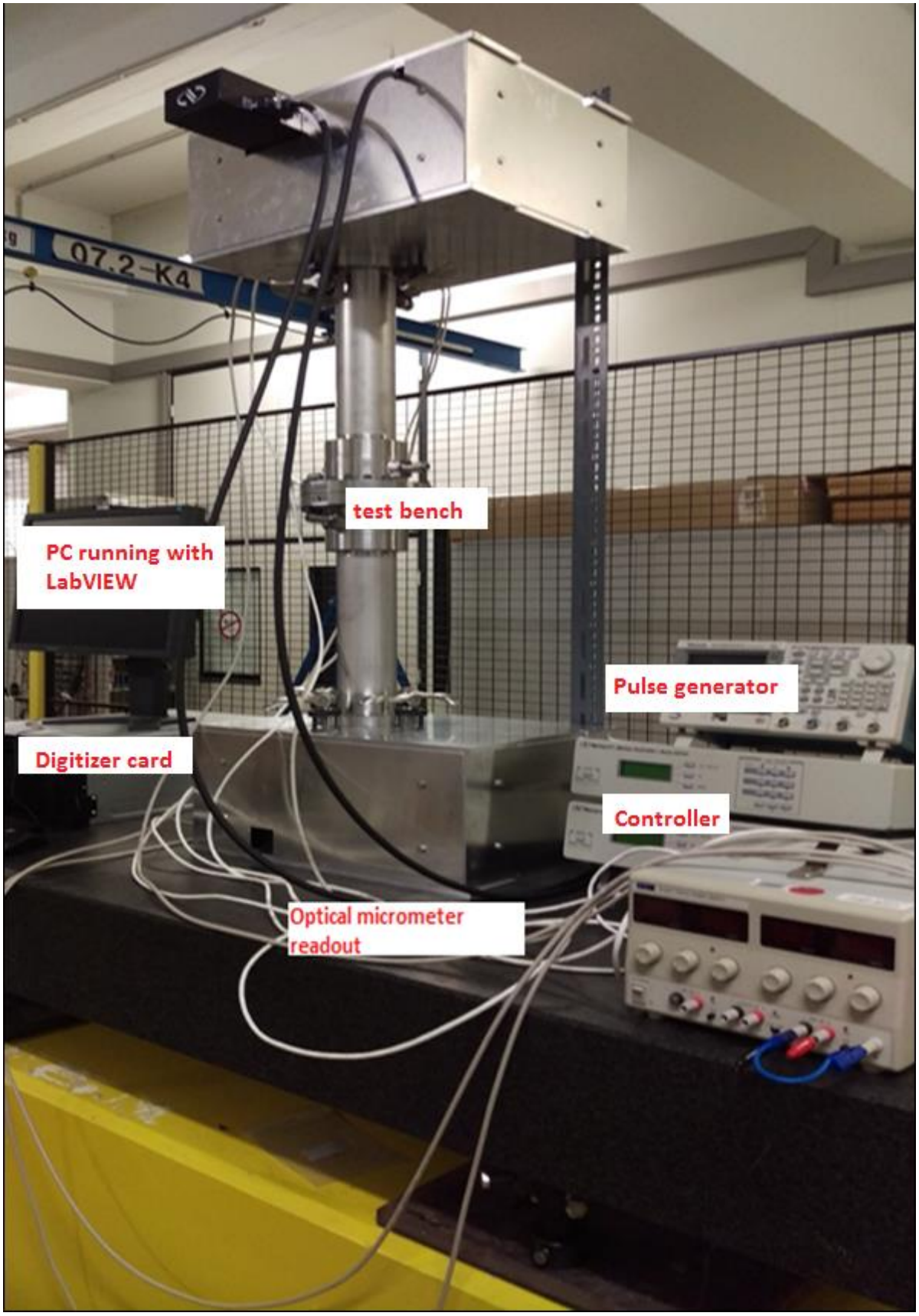

Figure 26: Complete setup for instrumentation equipment.

4.3. Test bench control and DAQ LabVIEW application

Figure 27 and Figure 28 shows the snapshot of the front panels of the LabVIEW application. This application was specifically written for automatizing the test bench control and DAQ of the characterization test setup. For the motion control of linear drives, grouping motion of the axes is preferred as it provides a synchronous motion of linear drives in X and Y direction. Figure 29 represents a snapshot of projected wire trajectories with respect to the beam pipe aperture. The step for every consecutive motion is 2 mm from -10 mm to +10 mm which is the center region of the beam pipe.

Figure 27: Front panel of the LabVIEW application for linear drive control. The Individual axis Home defines the wire positioning at the absolute mechanical center of the BPM. The spreadsheet path link to programmed mechanical sweep positions. The graphs are indications of performed group motion by master and slave groups. The master group motion is indicated as a negative slope as the two linear drives are placed pointing in opposite directions.

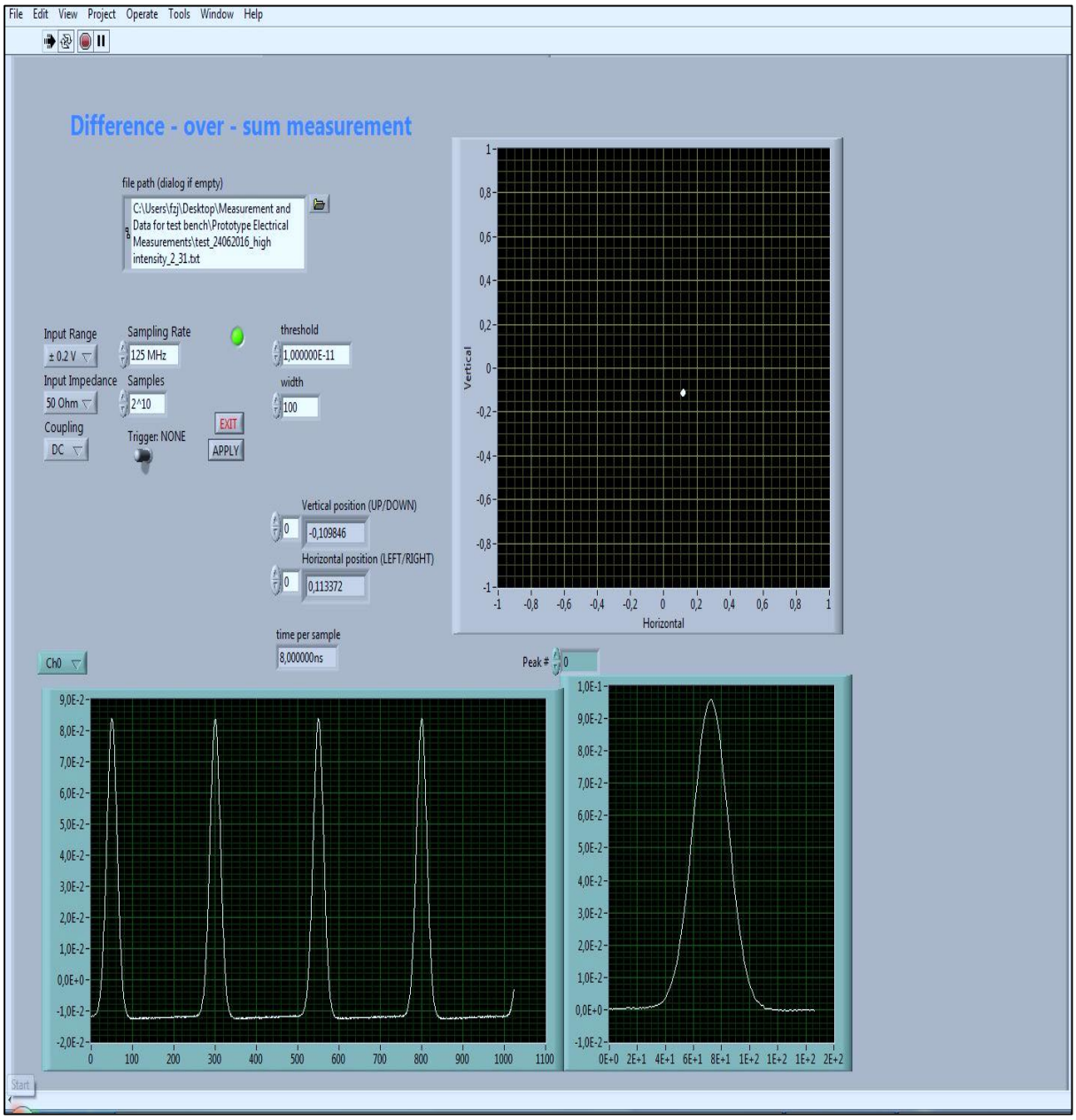

Figure 28: Front panel of the LabVIEW application for digitizer card. The upper right graphical window represents Horizontal DOS and Vertical DOS. The lower left window represents the waveform detected by the electrodes for one particular channel. The lower right window represents a single peak from the waveform after offset correction.

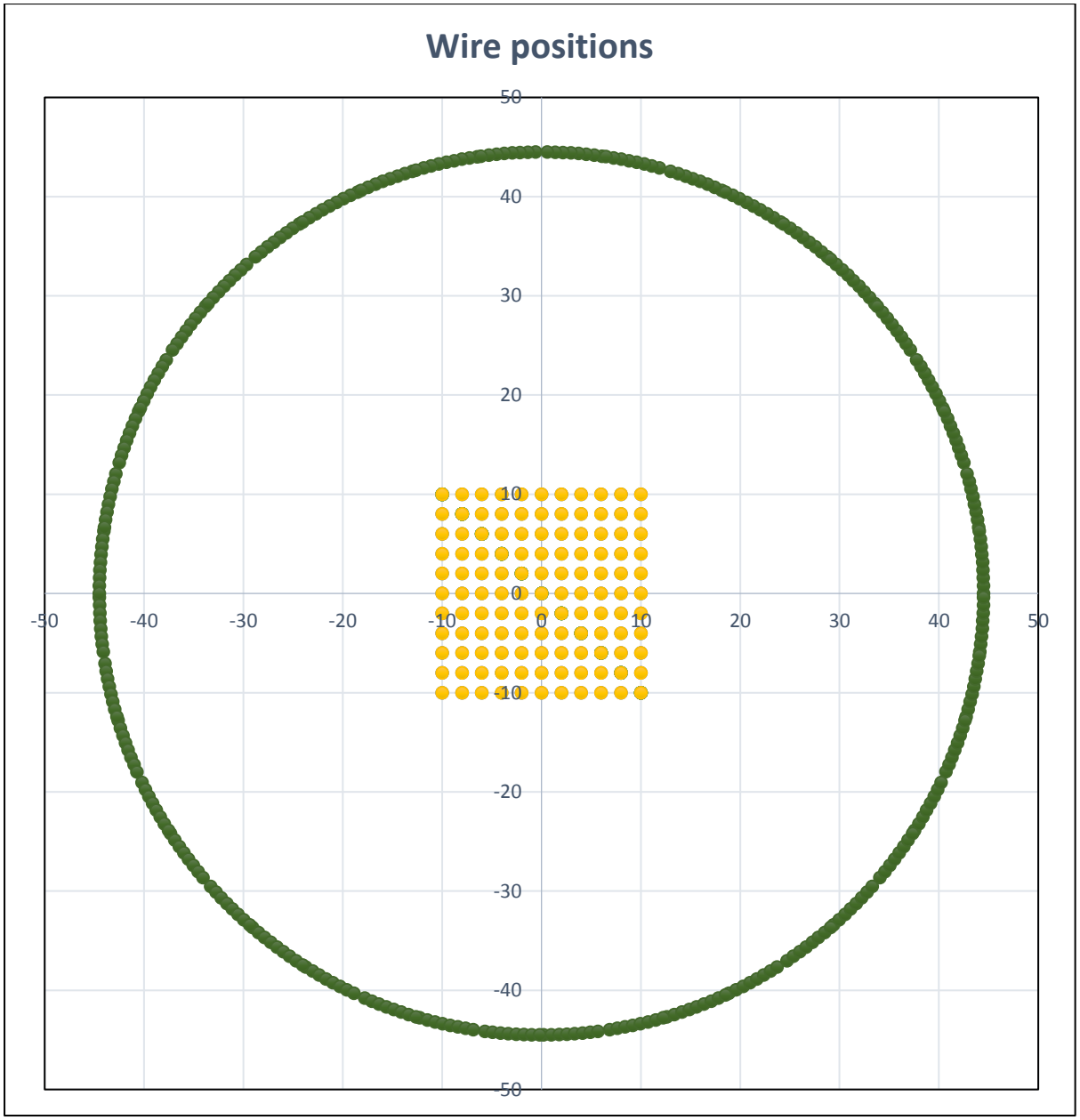

Figure 29: Wire positions for linear drive motion from (10, 10) to (-10, -10) through a zig-zag pathway (colored yellow) with 2 mm steps where the circular line represents the beam pipe aperture.

4.4. Linearity test configuration

Linearity tests were carried out with two test configuration. For both tests, a Gaussian signal is fed from a function generator directly to the wire terminal at the bottom reference. For the first test, the signal was matched to 10^{10} antiprotons within a bunch length of 172 m. This corresponds to a sigma (σ) of $98.5 \cdot 10^{-9}$s and a current of 6.5 mA over the wire. For the second test, the number of particles considered was 10^{8}. This corresponds to a current of 65 μA over the wire but with the same signal properties. With these signal parameters, a real beam was

simulated with the copper wire. The wire's Ohmic resistance is 0.559 Ω corresponding to its length of 1.04 m and diameter of 0.4 mm.

The four (V_+, V_-, H_+, H_-) BPM electrode outputs are then connected to the digitizer card via COSY BPM [24] amplifiers with a gain of 13.5 dB. The signal acquisition of the digitizer card was set such that its maximum dynamic range can be covered. The two test configurations are summarized in Table 6.

Sl.No	**Parameters**	**High particle intensity**	**Low particle intensity**
1	Energy	3 GeV	3 GeV
2	Length of the bunch	172 m	172 m
3	Number of particles	10^{10}	10^{8}
4	Beam current in A	$6.5*10^{-3}$	$6.5*10^{-5}$
5	Length of wire	1.04 m	1.04 m
6	Diameter of wire	0.4 mm	0.4 mm
7	Voltage across wire	4.2 V	42 mV
8	Amplification	13.5 dB	53.5 dB

Table 6: Signal input conditions for linearity tests configurations.

For low particle intensity i.e. 10^8 particles, an extra amplifier was used (FEMTO Messtechnik GmbH amplifiers: amplification gain of 40 dB) in order to maximize the use of the digitizer card's dynamic range.

5. Characterization test results and discussions

The linearity test confirms the linear response of the HESR BPM prototype as explained in 2.7, determines the sensitivity, and the accuracy that can be expected for 10^8 and 10^{10} antiprotons circulating in the ring.

5.1. Linearity test results

The linearity tests were carried out to obtain position sensitivity of the pickup S_V and S_H in both vertical and horizontal planes. It is represented as the slope of the linear fit according to the inverse of the linear approximation equations (38) and (39) which are confirmed by means of the optical micrometer assembly. With the same measurements the wire electrical offsets in horizontal and vertical planes as the intercept of the linear fit equations (36) and (37) can be calculated.

The procedures followed for the linearity test were as described in section 4.4 with positional sweeps in the range of ±10 mm with step sizes of 2 mm. In addition, the wire offset was corrected for every positions as suggested in section 3.2.2.

10^{10} particle intensity

For the first test configuration, the results for sensitivity in horizontal and vertical planes as corresponding slopes in Figure 30 and Figure 31 are presented.

$$S_H = (1.318 \pm 0.003)\ \%/mm$$

$$S_V = (1.330 \pm 0.003)\ \%/mm$$

Figure 32 represent electrical positions of the wire for corresponding mechanical positions translated through linear drives due to S_H and S_V. Figure 33 and Figure *34* represents the positional uncertainty distribution in horizontal and vertical planes due to S_H and S_V. $EOS_{H,V}$ represents electrical offset in horizontal and vertical directions.

$$EOS_H = 0.2135 \pm 0.0115\ mm$$

$$EOS_V = 0.9402 \pm 0.0107\ mm$$

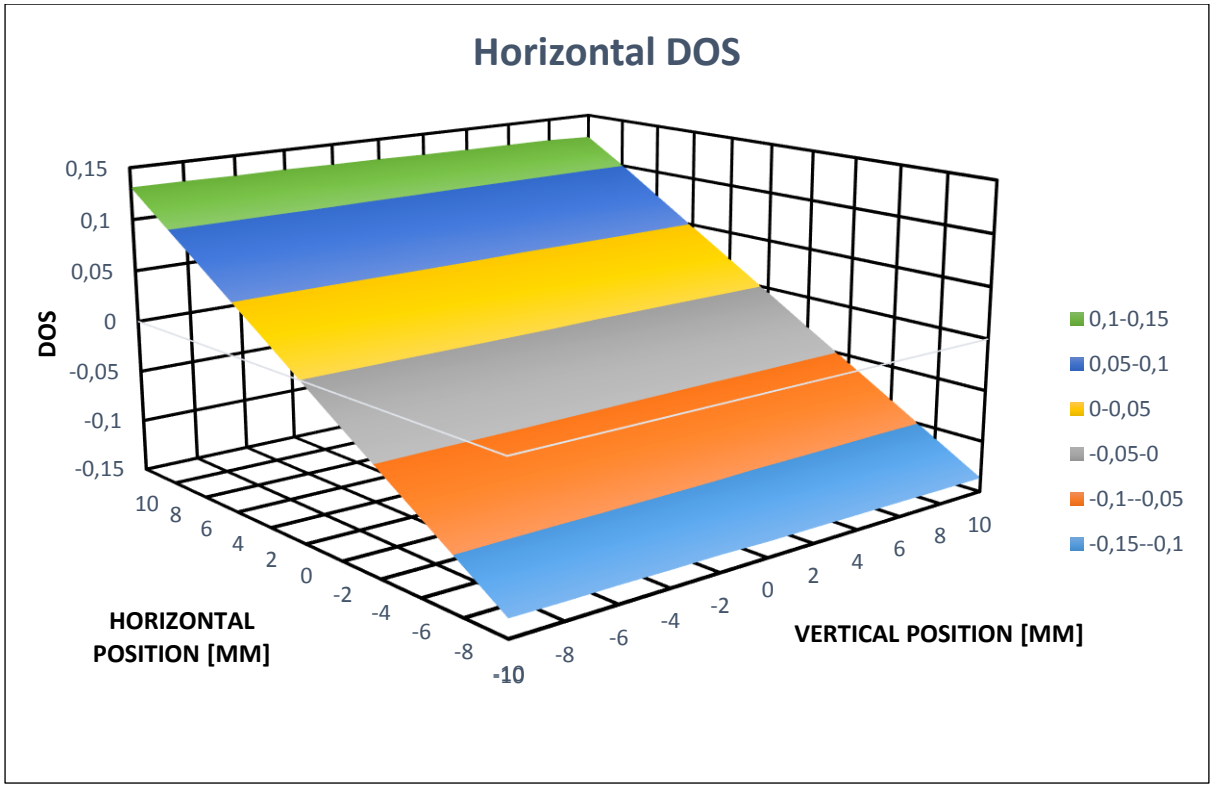

Figure 30: Distribution of difference over sum ratio (DOS) in the horizontal plane for all sweep positions i.e. ±10 mm with 2 mm steps.

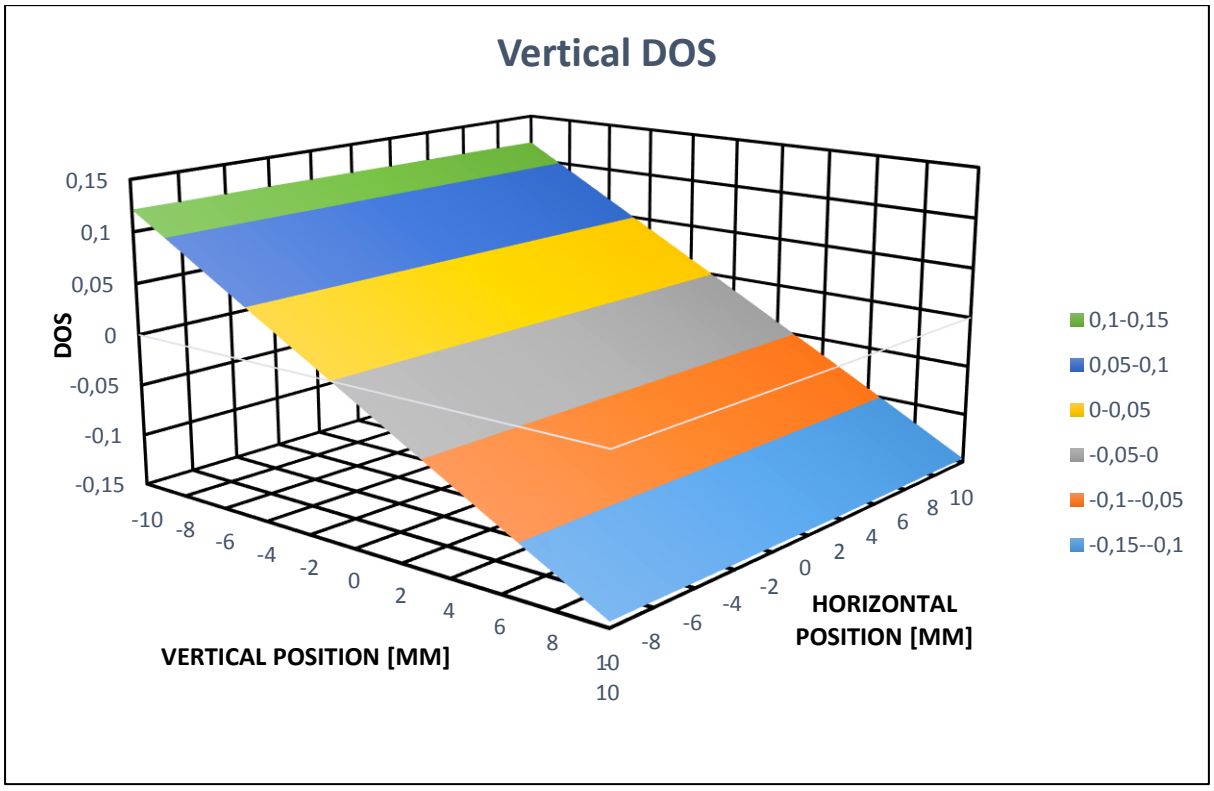

Figure 31: Distribution of difference over sum ratio (DOS) in the vertical plane for all sweep positions i.e. ±10 mm with 2 mm steps.

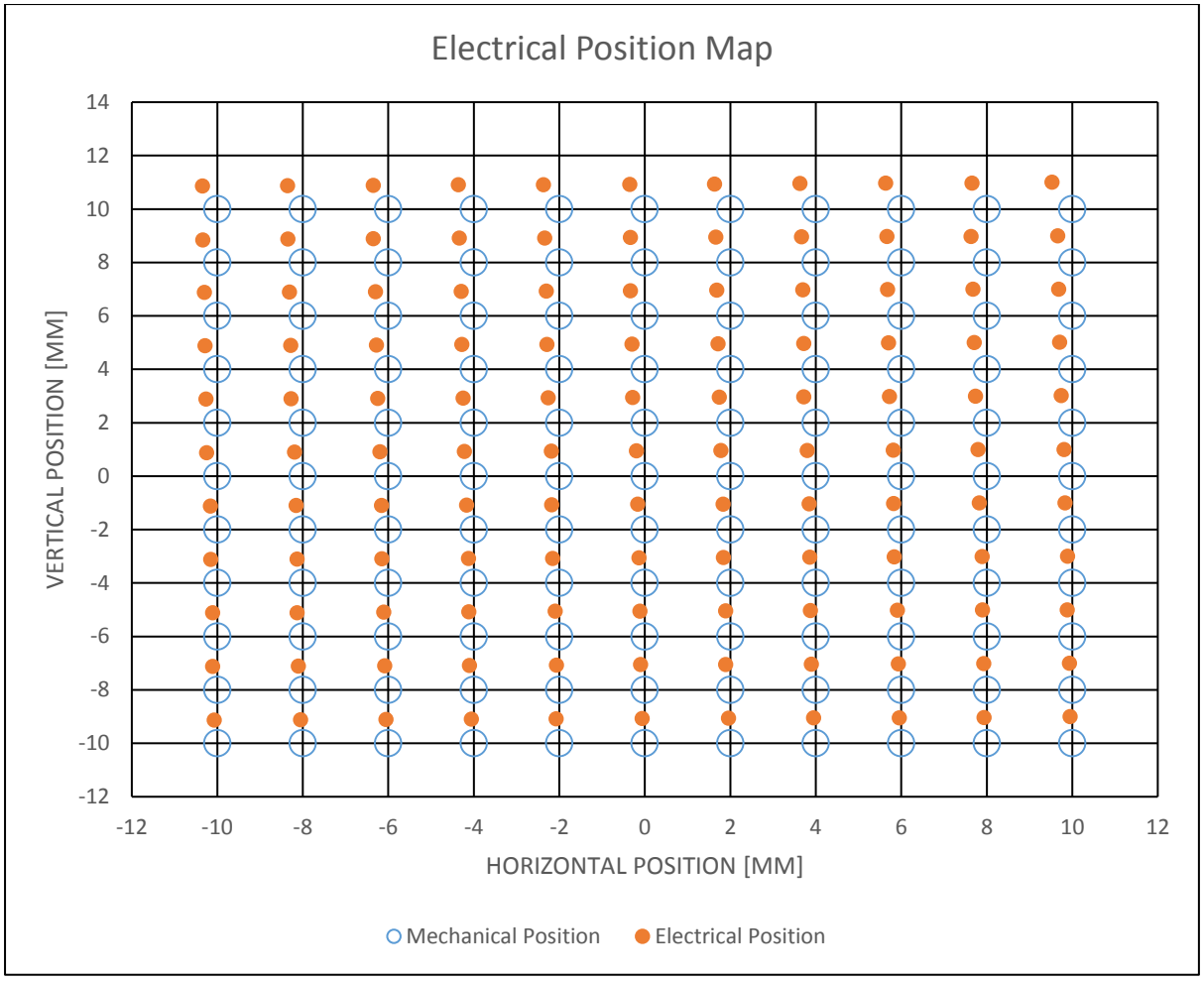

Figure 32: Electrical positions of the wire for corresponding mechanical positions considering both S_H and S_V.

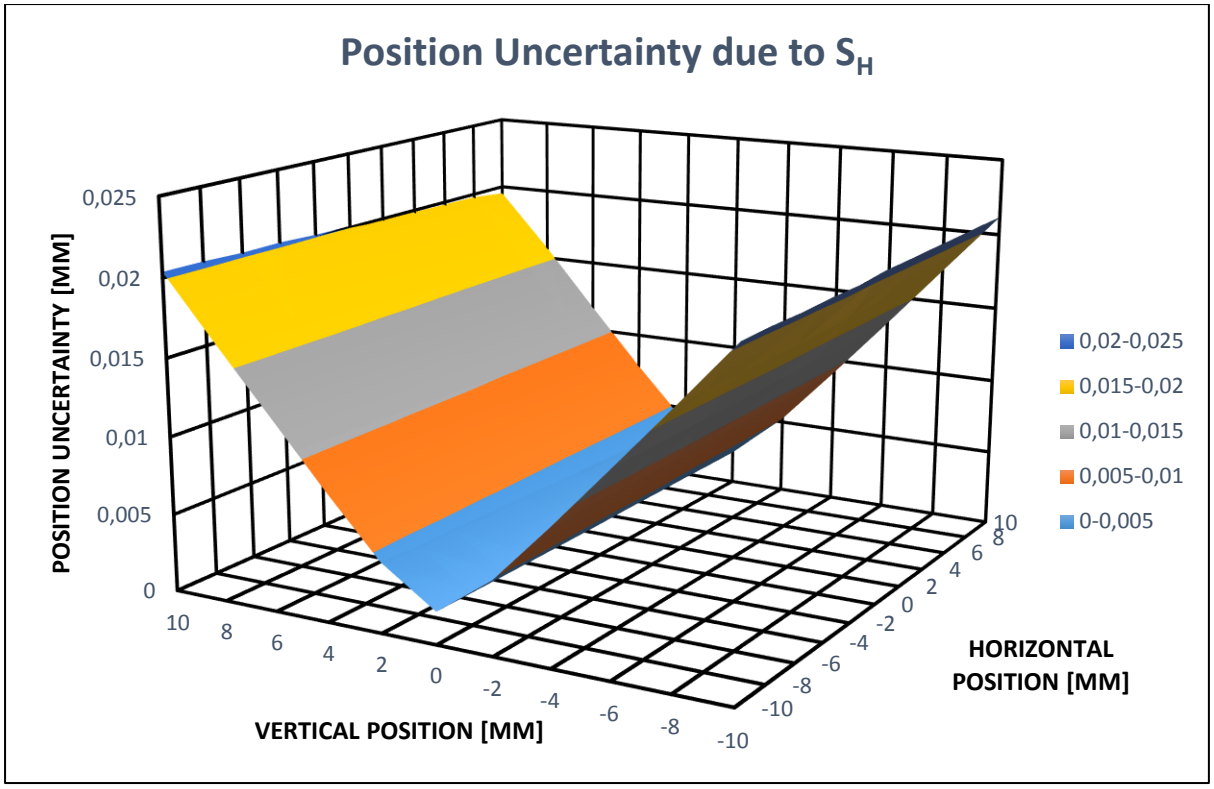

Figure 33: Linearity error distribution across positional sweeps of ±10 mm with 2 mm steps due to S_H.

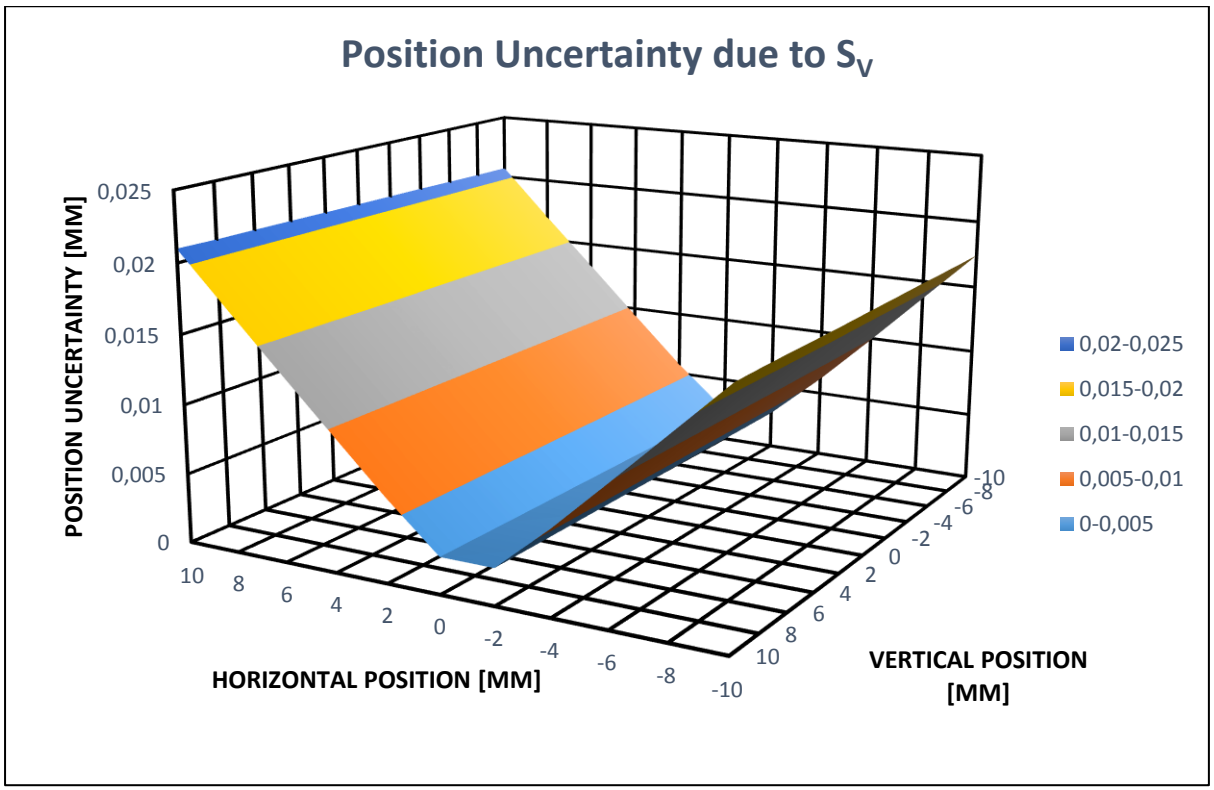

Figure 34: Linearity error distribution across positional sweeps of ±10 mm with 2 mm steps due to S_V.

10^8 particles intensity

For the second test configuration i.e. 10^8 particles, the results for sensitivity in horizontal and vertical planes as corresponding slopes in Figure 35 and Figure 36 are presented.

$$S_H = (1.312 \pm 0.058)\ \%/mm$$

$$S_V = (1.352 \pm 0.060)\ \%/mm$$

Figure 37 represent electrical positions of the wire for corresponding mechanical positions translated through linear drives due to S_H and S_V. Figure 38 and Figure *39* represents the positional uncertainty distribution in horizontal and vertical planes due to S_H and S_V. $EOS_{H,V}$ represents electrical offset.

$$EOS_H = 0.454 \pm 0.255\ mm$$

$$EOS_V = 1.841 \pm 0.262\ mm$$

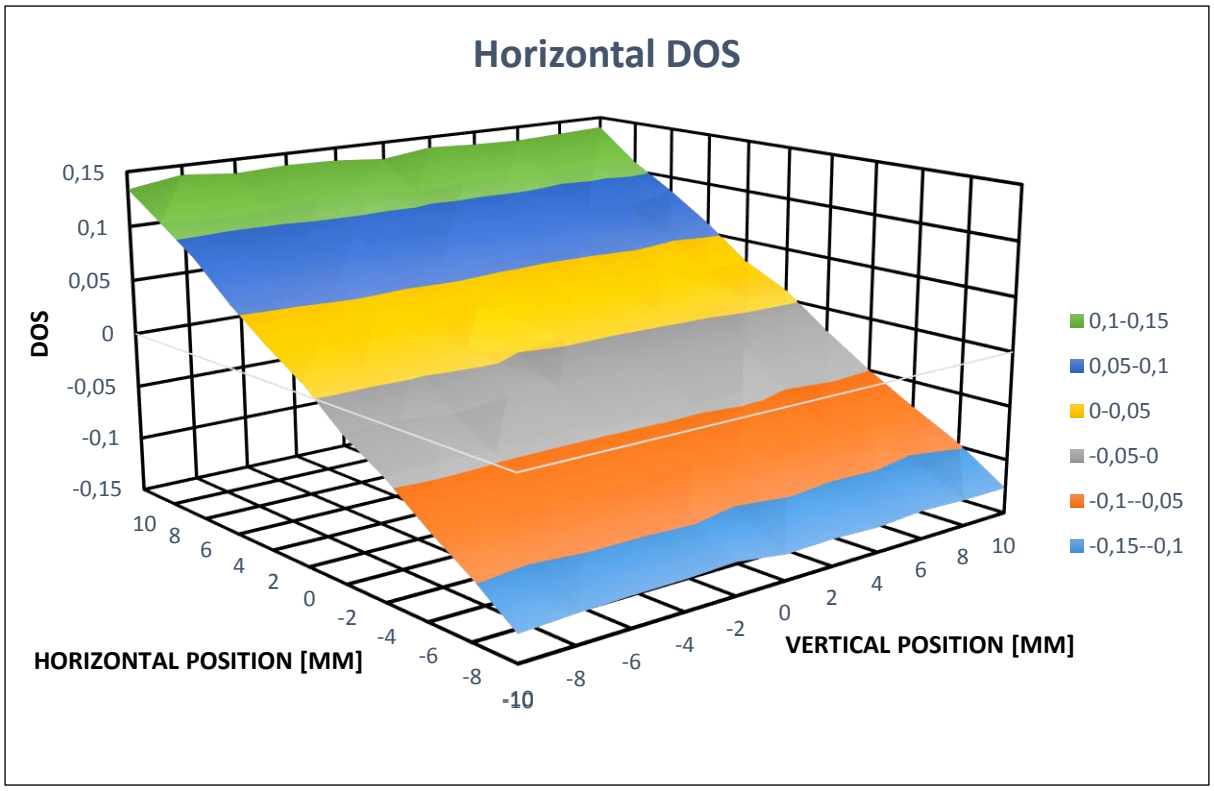

Figure 35: Distribution for difference over sum ratio (DOS) in the horizontal plane for all sweep positions i.e. ±10 mm with 2 mm steps.

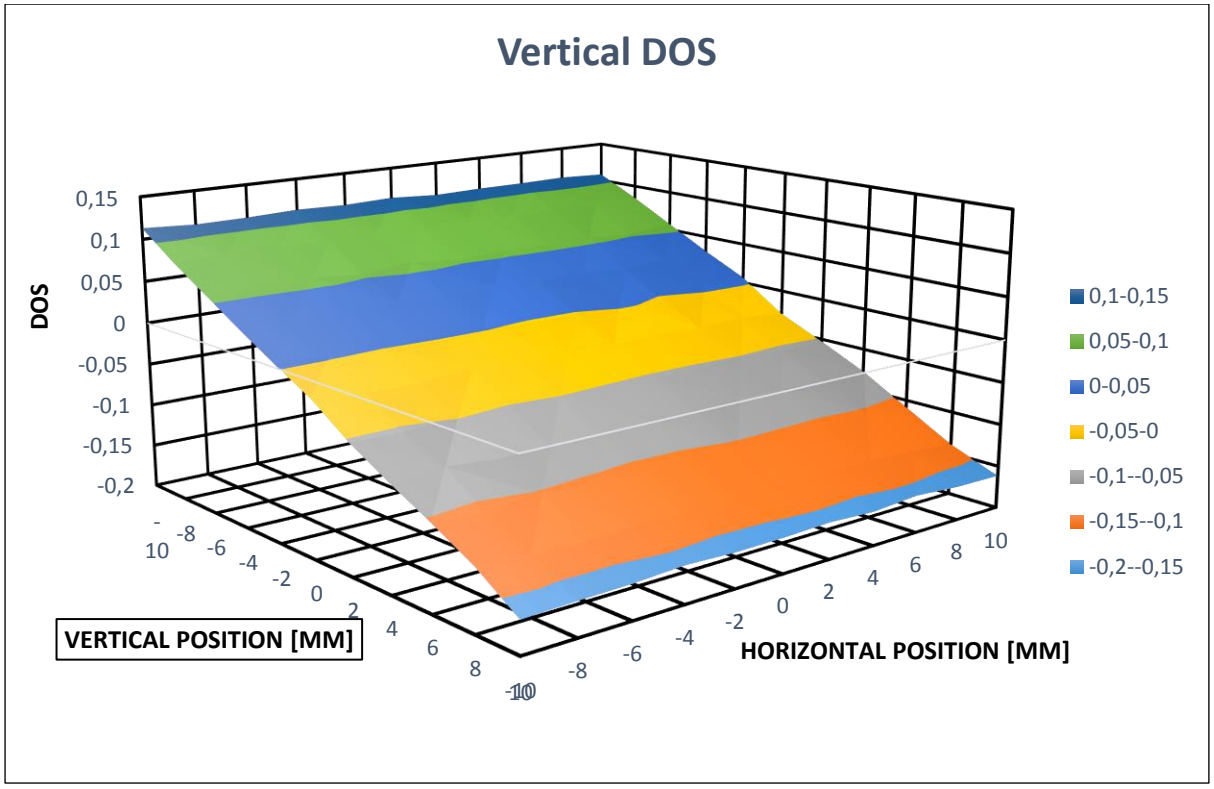

Figure 36: Distribution for difference over sum ratio (DOS) in the vertical plane for all sweep positions i.e. 10 mm with 2 mm steps.

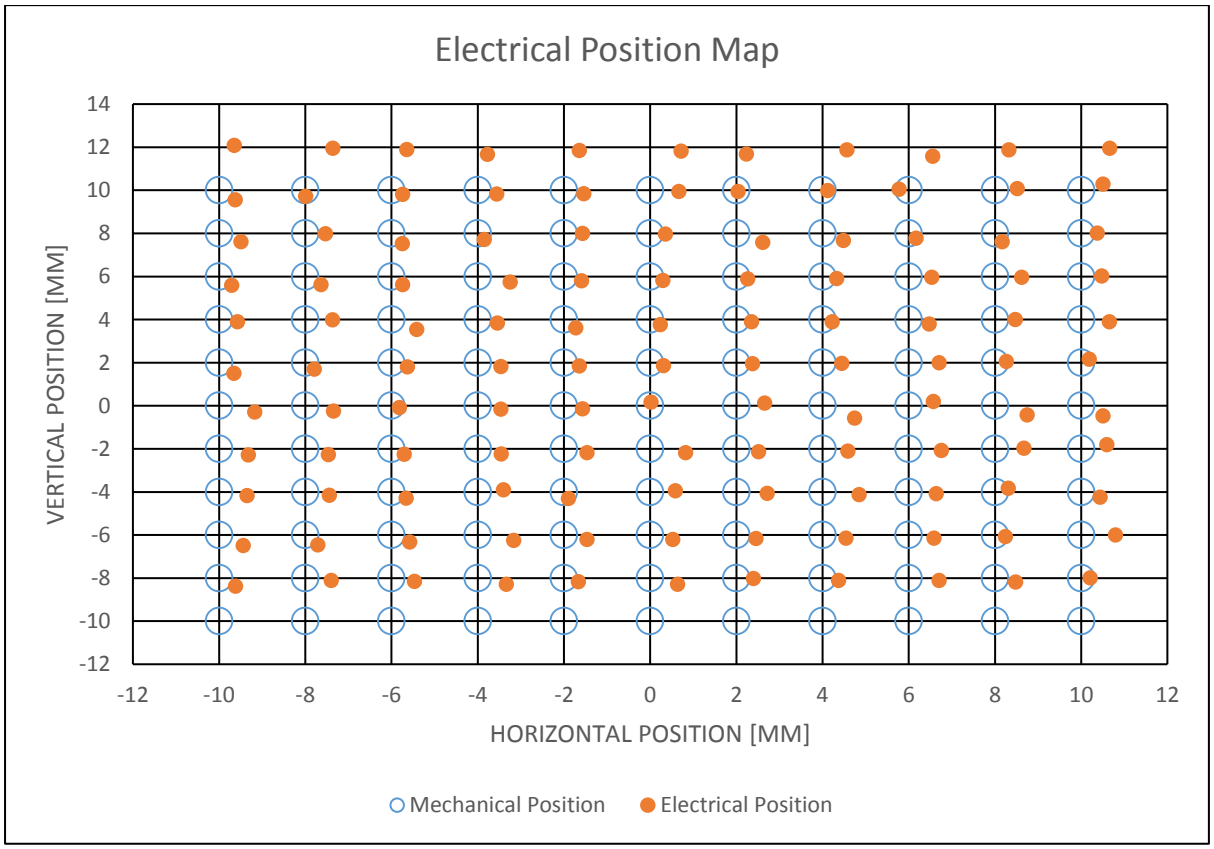

Figure 37: Electrical positions of the wire for corresponding mechanical positions considering both S_H and S_V.

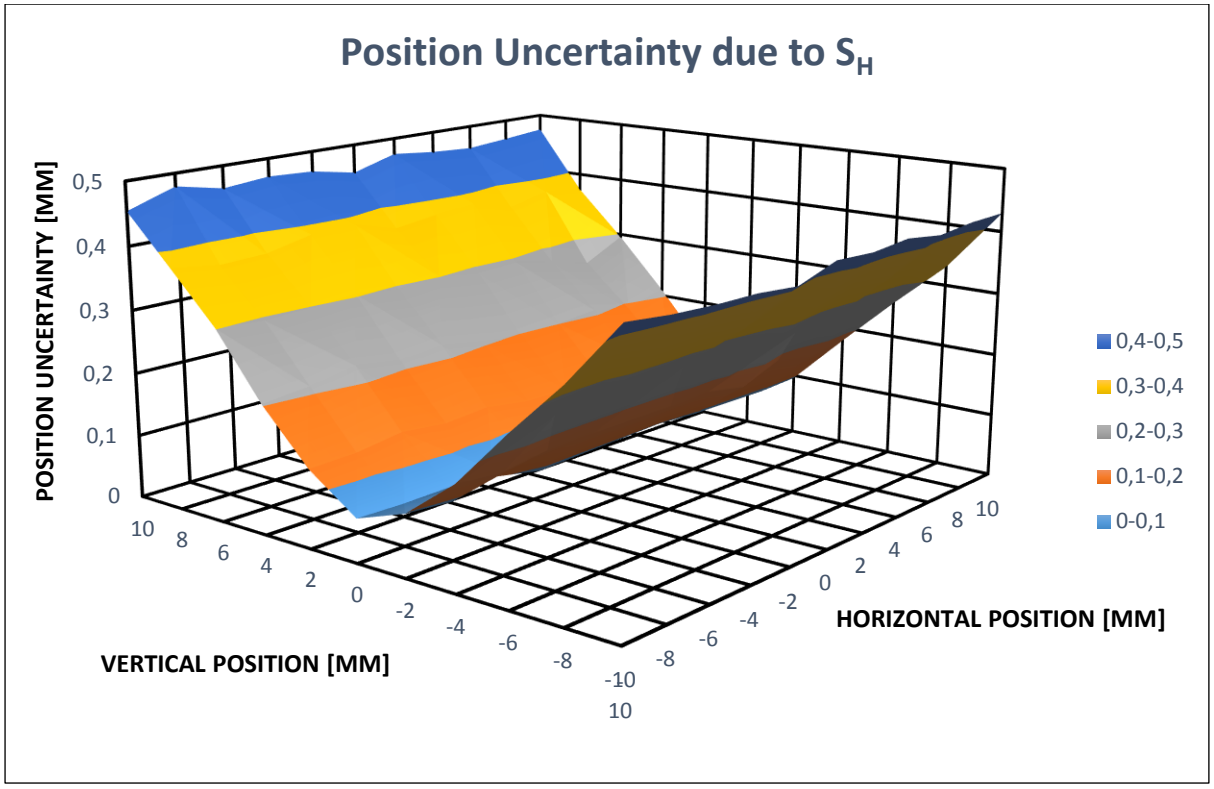

Figure 38: Linearity error distribution across position sweeps of ±10 mm with 2 mm steps due to S_H.

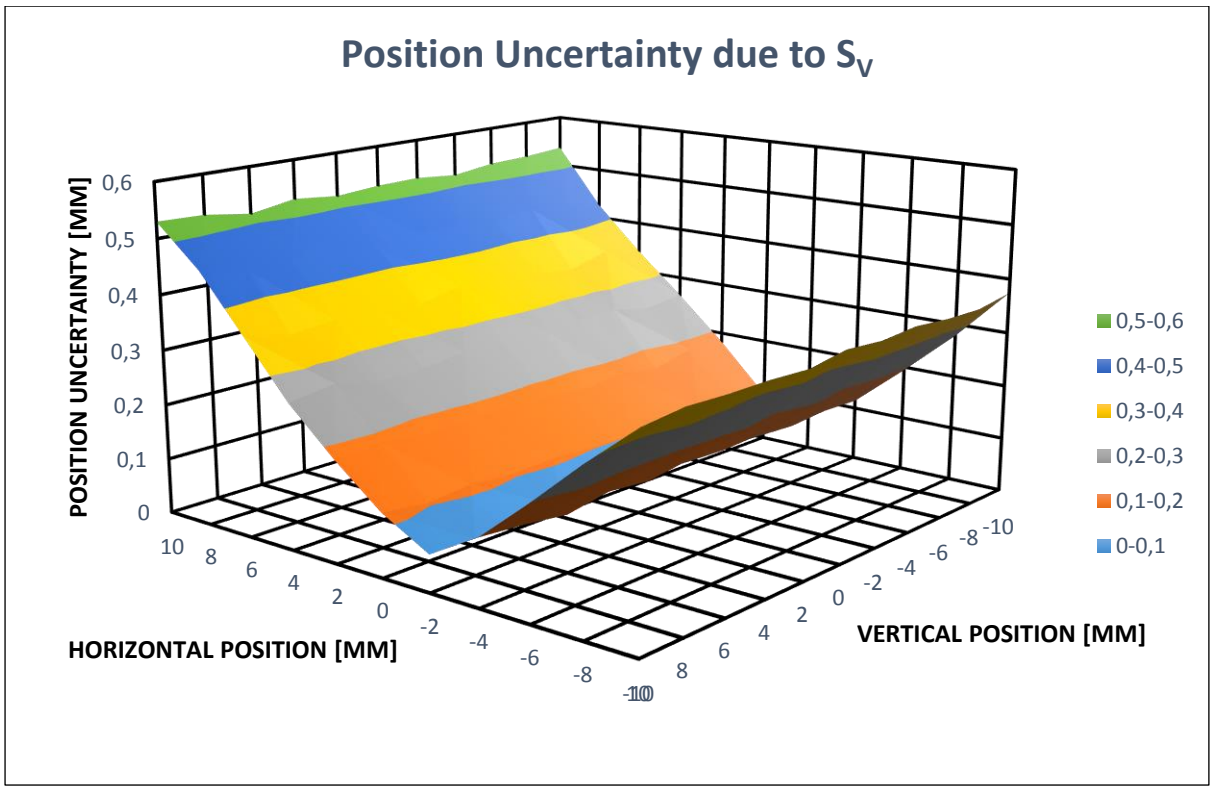

Figure 39: Linearity error distribution across position sweeps of ±10 mm with 2 mm steps due to S_V.

5.2. Discussion

The positional sensitivity i.e. $S_{H,V}$ and electrical offset that was measured in both the horizontal and vertical directions are not the same. This is because the BPM installation might be non-symmetric for both the directions and depending on the BPM surrounding, the propagation of the beam's electro-magnetic field might get modified. The non-symmetric installation of the individual electrodes was confirmed by the ZEA as there were fabrication issues while manufacturing the BPM prototype. In addition, a frequency dependence of the position sensitivity and electrical offset is possible due to the capacitive coupling.

The simulated position sensitivity for the BPM prototype in both the horizontal and vertical direction is 1.004 %/mm [25]. This corresponds to an individual electrode capacitance of 30 pF and connected in parallel was the COSY BPM amplifier with a capacitance of 10 pF. The sensitivity that was measured for the actual setup is higher by 30% approximately than the simulated value. This could be attributed to the non-symmetric actual individual electrode capacitances as shown in 4.1. Also could be the influence of the capacitive coupling between the adjacent electrodes and a reduction in the electrode's cross-talk. The actual value of the cross-talk could be much lower than the simulated value i.e. 8 pF [25]. The actual drop in cross-talk means the individual electrode capacitance could be higher than the measured value which could correspondingly increase the position sensitivity by a factor of 30%. Figure 40 represents positional sensitivity dependence with respect to additional amplifier capacitances [25] which justifies the explanation. However, the reasons attested have to be confirmed with further practical tests as well as a more detailed model for simulation has to be worked out with the findings of the test bench measurement.

In general, the electrical offset i.e. the offset of the geometrical center with respect to the electrical center is defined by the condition when the difference voltage is zero. This is attributed to the field inhomogeneity which arises from the asymmetry of the electric field at the adjacent electrode edges. This asymmetry itself arises from the non-symmetry of the BPM electrodes in their respective planes.

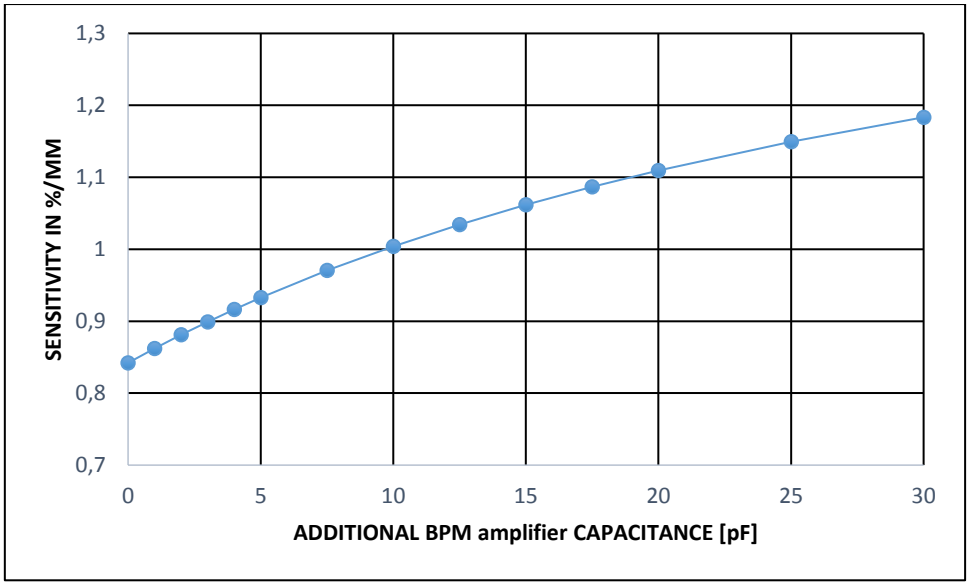

Figure 40: Dependency of sensitivity with additional capacitance in pF [25].

The offset can be minimized by reducing the field inhomogeneity by providing guard rings at ground potential from either ends to ensure identical environments. When guard rings are not provided as in the case of the BPM prototype, electrical offsets can be as large as 10% of the BPM half-aperture [16]. However, in the BPM prototype, the worst case electrical offset is only 4% of the BPM half-aperture.

The BPM performance is characterized by the overall precision σ_H and σ_V in measuring the beam absolute position in horizontal and vertical plane respectively. The overall precision is calculated as the root mean square of the linearity errors at wire positions in the range of interest i.e. ± 10 mm. For 10^{10} particles, the overall precision in both horizontal and vertical coordinates are

$$\sigma_H = 13.1\ \mu m \text{ and } \sigma_V = 12.3\ \mu m$$

which is within the requirements of the BPMs for HESR i.e. 100 µm. For 10^8 particles, the overall precision in both horizontal and vertical coordinates are

$$\sigma_H = 0.286\ mm \text{ and } \sigma_H = 0.297\ mm$$

Which is also within the requirements of the BPMs i.e. 1 mm.

Regarding the test bench mechanical tolerance, the granite slab would minimize such intolerances of the final assembly. The metrological inspection of the working components of the test bench accredits this situation. Besides these mechanical intolerances, electronic properties like amplifier gain errors, noise and

electromagnetic interferences can also influence the accuracy. The amplifier gain errors can be compensated by calibrating the electronics regularly. In addition, digitalization escorts to granularity of values which might limit the reachable accuracy.

In any electronic circuit, the presence of electrical noise is a common source of uncertainty. This noise may be due to external influences as mentioned earlier. Proper shielding techniques and electrical design can minimize the severity of uncertainty due to noise. This can be achieved by using low noise amplifiers in order to match the signal level. However, the COSY BPM amplifiers that are used for the measurement have a high input impedance due to the demand for having a low cut-off frequency. A trade-off between low cut-off frequency and thermal noise has to be taken into consideration.

The signal acquisition settings that was set on the digitizer card for 10^{10} and 10^{8} particle intensity is shown in Table 7. The number of bunches acquired for averaging signals is few with such acquisition settings. Therefore it is fairly straightforward to say that increasing the number of bunches for averaging would reduce the measurement uncertainty as the standard deviation is inversely proportional to the square root of the number of bunches.

Signal Acquisition parameters	**Value**	**Unit**
Sample Rate	$6.25*10^{7}$	S/s
Revolution frequency	$5.00*10^{5}$	Hz
Sample per bunch	125.00	S
Time per bunch	$2.00*10^{-6}$	s
Recorded samples	65536	S
Acquired bunches	524	1
Time per sample	$1.60*10^{-8}$	s

Table 7: Signal acquisition settings for the digitizer card for 10^{10} and 10^{8} particle intensity

However, if the noise signal is not random, using appropriate filters is an option [26]. Filtering the signal will consequently reduce the bandwidth which will significantly reduce the noise and improve the sensitivity to small signals.

The characterization parameters results for 10^{10} and 10^{8} particle intensity are shown in Table 8 and Table 9.

BPM Linearity test parameters for 10^{10} particles	
Position Sensitivity	
Horizontal, S_H	$(\mathbf{1.318 \pm 0.003})\ \%/\boldsymbol{mm}$
Vertical, S_V	$(\mathbf{1.330 \pm 0.003})\ \%/\boldsymbol{mm}$
Electrical Offset	
Horizontal, EOS_H	$\mathbf{0.2135 \pm 0.0115}\ \boldsymbol{mm}$
Vertical, EOS_V	$\mathbf{0.9402 \pm 0.0107}\ \boldsymbol{mm}$
Linearity Error	
Horizontal	$\mathbf{0.0115 \pm 0.0062}\ \boldsymbol{mm}$
Vertical	$\mathbf{0.0107 \pm 0.0059}\ \boldsymbol{mm}$
Overall Precision (RMS)	
Horizontal, σ_H	$\mathbf{13.1}\ \boldsymbol{\mu m}$
Vertical, σ_V	$\mathbf{12.3}\ \boldsymbol{\mu m}$

Table 8: BPM linearity test parameter with their corresponding uncertainty for 10^{10} particle intensity

BPM Linearity test parameters for 10^{8} particles	
Position Sensitivity	
Horizontal, S_H	$(\mathbf{1.312 \pm 0.058})\ \%/\boldsymbol{mm}$
Vertical, S_V	$(\mathbf{1.352 \pm 0.060})\ \%/\boldsymbol{mm}$
Electrical Offset	
Horizontal, EOS_H	$\mathbf{0.454 \pm 0.255}\ \boldsymbol{mm}$
Vertical, EOS_V	$\mathbf{1.841 \pm 0.262}\ \boldsymbol{mm}$
Linearity Error	
Horizontal	$\mathbf{0.255 \pm 0.130}\ \boldsymbol{mm}$
Vertical	$\mathbf{0.262 \pm 0.141}\ \boldsymbol{mm}$
Overall Precision (RMS)	
Horizontal, σ_H	$\mathbf{0.286}\ \boldsymbol{mm}$
Vertical, σ_V	$\mathbf{0.297}\ \boldsymbol{mm}$

Table 9: BPM linearity test parameter with their corresponding uncertainty for 10^{8} particle intensity

6. Conclusion and Future works

For beam diagnostics in hadron machines, diagonal cut capacitive pickup (BPM) is a device of choice due to its high linear behavior and high sensitivity. However, prior to any beam operation, it is essential to characterize the BPM. This involves substantiating a relationship between beam position and position sensitivity by performing linearity characterization test. This was accomplished with the aid of a stretched wire test bench.

The design of the test bench had to take into consideration mechanical tolerances and alignment errors which can consequently affect measurement accuracy. The fundamental design concept is the in-tower mounting of the BPM along with its main stand elements within two BPM reference boxes as explained in 3.2.1. Such a design is preferred in order to accommodate BPM assembly of varying lengths for characterization tests. This also aids in realization of the stretched wire passing through the hollow center of the BPM, thus avoiding any wire bending due to gravity. Moreover, the optical micrometer assembly provides online metrological inspection which mitigates wire alignment errors as it is placed at BPM's mechanical home with respect to the reference pins. Concerns of alignment errors and deformation under load was allayed with the stress analysis which proved that maximum deformation under load does not exceed nanometers as explained in 3.2.2. The test bench was successfully constructed with the help of ZEA followed by the confirmation of the design. This test bench is developed with the idea to use it for series production of the BPMs thereby making it a versatile test bench. Accompanying the construction, was the development of a software that was used for automatization and for data acquisition to characterize the BPM.

Linearity characterization tests were performed on the BPM for two test conditions. One for high particle intensity i.e. 10^{10} particles and the other for low particle intensity i.e. 10^{8} particles. For both 10^{10} and 10^{8} particle intensities, the linearity behavior of the BPM could be confirmed successfully. The results indicate that the BPM could achieve positional accuracy in both horizontal and vertical plane within the requirements i.e. 100 µm (10^{10} particles) and 1 mm (10^{8} particles) for closed orbit measurement.

For 10^{10} and 10^{8} particle intensity, measurement uncertainties are greatly reduced with 524 acquired bunches for averaging.

Moreover, for approving the series production of HESR BPMs, single turn detection measurement will be carried out on the test bench (both as sum and difference signal).

Bibliography

[1] W. Panofsky, "Evolution of Particle Accelerators," *Slac.Stanford.Edu*, 1997.

[2] O. Barbalat, "Applications of Particle Accelerators," 1994.

[3] E. Clements, "New tools forge new frontiers," *Symmetry (Basel).*, vol. 05, no. 03, pp. 10–15, 2008.

[4] R. Maier and U. Pfister, "COSY -JULICH A SYNCHROTRON AND STORAGE RING FOR MEDIUM ENERGY PHYSICS," in *Proceedings of the 13th International Conference on Cylotrons and their Applications, Vancouver, BC, Canada*, 1992, pp. 282–285.

[5] M. Steck, "Beam Cooling," *Cern Accel. Sch.*, 2011.

[6] "FAIR Baseline Technical Report," 2006.

[7] B. Gålnander, S. Johnson, T. Johnson, and et.al, "HESR AT FAIR : STATUS OF TECHNICAL PLANNING," in *Proceedings of PAC07, New Mexico, USA*, 2007, pp. 1442–1444.

[8] R. J. Maier, "THE HIGH-ENERGY STORAGE RING (HESR)," in *Proceedings of PAC11, New York, USA*, 2011, pp. 2104–2106.

[9] "PANDA." [Online]. Available: https://panda.gsi.de/oldwww/.

[10] "SPARC: Atomic physics, quantum electrodynamics, ultra-high electro-magnetic fields studies with beams of highly-charged heavy ions." [Online]. Available: https://www.gsi.de/work/forschung/appamml/atomphysik/forschung/ap_und_fair/sparc/einleitung.htm. [Accessed: 22-Jul-2016].

[11] "PAX Collaboration." [Online]. Available: http://collaborations.fz-juelich.de/ikp/pax/about/introduction.shtml. [Accessed: 22-Jul-2016].

[12] A. Lehrach, B. Lorentz, R. Maier, D. Prasuhn, and et.al, "BEAM DYNAMICS STUDIES FOR THE HIGH-ENERGY STORAGE RING *," in *Proceedings of ICAP 2006, Chamonix, France*, 2006, no. 515873, pp. 96–101.

[13] H. Koziol, "Beam diagnostics for accelerators," *CAS - Cern Accel. Sch. Basic Course Gen. Accel. Phys.*, pp. 1–44, 2005.

[14] P. Forck, "Lecture Notes on Beam Instrumentation and Diagnostics," *Jt. Univ. Accel. Sch.*, pp. 0–152, 2011.

[15] E. Bravin, "Transverse Beam Profiles," *Cern Accel. Sch. Beam Diagnostics*, pp. 377–406, 2009.

[16] P. Forck, P. Kowina, and D. Liakin, *CERN Accelerator School Beam Diagnostics*. CERN EUROPEAN ORGANIZATION FOR NUCLEAR RESEARCH, 2009.

[17] R. E. Shafer, "Beam Position Monitoring," *AIP Conf. Proc.*, vol. 212, pp. 26–58, 1990.

[18] J. J. G. Garrigos, "Development of the Beam Position Monitors for the Diagnostics of the Test Beam Line in the CTF3 at CERN," Universitat Politecnica de Valencia, 2013.

[19] M. Žnidarčič, *Libera Hadron User Manual*, First Edit. 2016.

[20] W. Kaufmann, "Amplifier for beam position monitors," 2012.

[21] *RIFTEK PRODUCT CATALOG*. Rifktek, 2015.

[22] "User Manual M-ILS150HA." [Online]. Available: http://www.newport.com/ILS-Series-High-Performance-Mid-Range-Travel-Line/140110/1033/info.aspx. [Accessed: 01-May-2016].

[23] *ESP 301 User's manual*. Newport, 2003.

[24] "BPMeP Vorverstärker," 1992.

[25] A. Halama (Forschungszentrum Jülich/IKP-4), *Private Communications*. .

[26] Bryan Peterson (Brigham Young University), "Physics 240: Design, Fabrication and Use of Scientific Apparatus," 2016, pp. 95–109.

List of Figures

List of Tables